INTERNATIONAL ATOMIC ENERGY AGENCY

INDC(CCP)-441
Distr.: L0

I N D C INTERNATIONAL NUCLEAR DATA COMMITTEE

Articles Translated from Journal Yadernye Konstanty (Nuclear Constants)

(Series: Nuclear Constants, Issue No. 1, 2004)

Translated by the IAEA

November 2004

IAEA NUCLEAR DATA SECTION, WAGRAMER STRASSE 5, A-1400 VIENNA

Nuclear Data Section
International Atomic Energy Agency
P.O. Box 100
Wagramer Strasse 5
A-1400 Vienna
Austria

Produced by the IAEA in Austria
November 2004

INDC(CCP)-441
Distr.: L0

Articles Translated from Journal Yadernye Konstanty (Nuclear Constants)

(Series: Nuclear Constants, Issue No. 1, 2004)

Abstract

This report contains the translation of three papers published in the Nuclear Constants journal (Voprosy Atomnoj Nauki I Teknniki, seriya: Yadernye Konstanty (YK), vypusk 1, 2004).

November 2004

Contents

NEUTRON CONSTANTS AND PARAMETERS

NEUTRON CONSTANTS AND PARAMETERS

04-34911 [1]
Translated from Russian

UDC 539.125.5

DIFFERENTIAL CROSS-SECTIONS OF (p,n) REACTIONS FOR Sn, Pb and Bi ISOTOPES*

A.A. Lychagin, B.V. Zhuravlev, V.G. Demenkov
V.I. Trykova, V.K. Debin, V.I. Spirin, Yu.A. Chalyj

The differential cross-sections of (p,n) reactions for Sn, Pb and Bi isotopes were measured on a time-of-flight spectrometer based on the EhGP-15 accelerator at the Institute of Physics and Power Engineering (IPPE). Thanks to the thin foils of material used and high time resolution, good energy resolution was obtained. The measurements were made in the 7–11 MeV proton energy region for a 15–140° angular distribution.

Introduction

Experimental data on the differential cross-sections of interaction in (p,n) reactions are of interest both for establishing a consistent theoretical description of the mechanisms of nuclear reactions and the statistical characteristics of excited nuclei and for solving a number of practical problems related to space research and radioisotope production. This paper presents the results of measurements of the excitation functions, spectra and angular distributions of neutrons from (p,n) reactions on nuclei of the isotopes ^{116}Sn, ^{118}Sn, ^{124}Sn, ^{208}Pb and ^{209}Bi at proton energies of 7–11 MeV. Earlier experimental data for these isotopes [1–6] either do not meet current accuracy and resolution requirements for theoretical analysis or only give excitation function measurement results over a limited range of proton energies.

Experimental technique

The measurements were performed on a time-of-flight spectrometer [7–9] using the pulsed mode of the EGP-10M and EGP-15 accelerators to obtain the proton beam. Thanks to the upgrading of the accelerators' interruption and grouping systems, current pulses on the target approximately 1 ns in duration with a repetition rate of 1, 2.5 and 5 MHz could be obtained. One important result of the upgrade was that it is now possible to control the beam parameters directly from the workplace of the physicist conducting the experiment by the latter setting the required parameters in the measurement program or manually from the control panel. The interruption frequency, bunch duration, phase shift and grouping amplitude can be specified. All settings are monitored using a built-in digital voltmeter and a correction modes switch. A typical experiment geometry is shown in Fig. 1. The particle beam from the accelerator, passing along the ion guide through the focusing lenses (1), the lamellae (2) and the pick-up electrode (3), struck the target (4) made from the material being studied and passed on into the Faraday cylinder (5). To reduce the neutron and gamma-ray background, the bottom of the Faraday cylinder was clad with carbon on which the (p,n) reaction has a high threshold. Neutrons formed in the target as a result of (p,n) interaction are registered by the 'main' neutron detector (6) installed in the shielding made of paraffin wax mixed with lithium hydride. To reduce the gamma ray background from interaction of neutrons with the shielding materials and the environment, the detector was encased in a layer of lead up to 10 cm thick. A ∅40×40 mm stilbene crystal connected with an optical contact to an FEhU-143 photomultiplier was used as the main neutron detector. A second neutron detector (7) was used as a 'control' detector. This detector consisted of a BP-20 fast plastic scintillator and an FEhU-87 photomultiplier. The control detector was installed in the shielding made of paraffin wax mixed with lithium hydride. A lead insert was used to protect against gamma-ray background. The control detector

* This study was carried out with the support of the Russian Foundation for Fundamental Research and the Kaluga Scientific Centre (grant 04-02-97237).

was directed towards the bottom of the Faraday cylinder and mainly registered the gamma rays emitted from it. The zero-time point was taken from the pick-up electrode. The lamellae and the diaphragm installed in front of them were used to centre the particle beam along the axis of the ion guide. By using a six-position target holder we were able to measure five elements and the background without stopping the accelerator. The positions were switched remotely from the workplace of the operating physicist. Foils made of ^{116}Sn (97.8%), ^{118}Sn (98.7%), ^{124}Sn (97.5%), ^{208}Pb (98.3%) and ^{209}Bi (99.9%) 4.3, 5.0, 3.79, 4.2 and 7.79 mg/cm^2 thick, respectively were used as the targets.

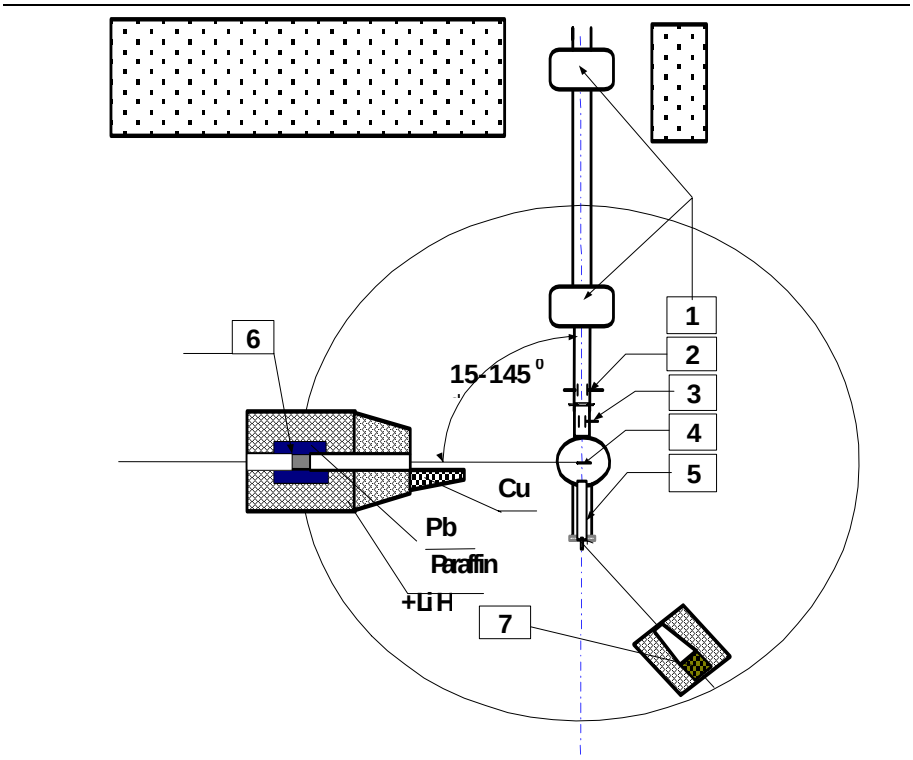

Fig. 1. Geometry of the experiment:

1 – focusing lenses, 2 – lamellae, 3 – pick-up electrode, 4 – target, 5 – Faraday cylinder, 6 – main neutron detector, 7 – control detector

The total time resolution in different measurement cycles varied from 0.5 to 0.8 ns/m. The range of measurable angles was 15–145^o and the time base was 259 cm. Since the initial proton energy varied during the measurement process, as did the mean energy depending on the foil thickness and material, specific values for the latter are given in the information section on the data obtained. The angles at which the various measurements were performed are given in the same place.

To determine the number of protons striking the target, a current integrator was used to measure the total charge delivered by the beam to the bottom of the Faraday cylinder over the measurement time. The current integrator was also used as the main monitor. The number of protons lost through interaction with the foil made of the material to be studied was disregarded. The design of the Faraday cylinder, which was 300 mm long with an entrance window 40 mm in diameter, virtually prevented charge leakage. The operational stability of the current integrator was checked from the stabilized current source. After one hour's warm, the mean-square deviation of the results of measurements lasting 30 mins over the course of 48 hours did not exceed 0.8% for a current source stability of 0.1%. This check was repeated periodically throughout the measurement cycle. The results of all checks were similar to the data given.

A block diagram of the electronic equipment is given in Fig. 2.

The efficiency of the main neutron detector (Fig. 3) was determined by measuring ^{252}Cf spontaneous fission neutron spectra and comparing them with the spectrum adopted as the standard [10]. The efficiency

was measured periodically at the start and end of each week or measurement cycle. The results of individual measurements coincided to within the limits of statistical error and so the time spectra were summed to reduce this. The curve line shows the result of describing the experimental points using two Legendre polynomials: one was used in the neutron energy range from the threshold to 1.5 MeV and the other from 1.5 to 10 MeV. The neutron detection threshold was ~200 keV for a gamma-ray rejection ratio of approximately 20.

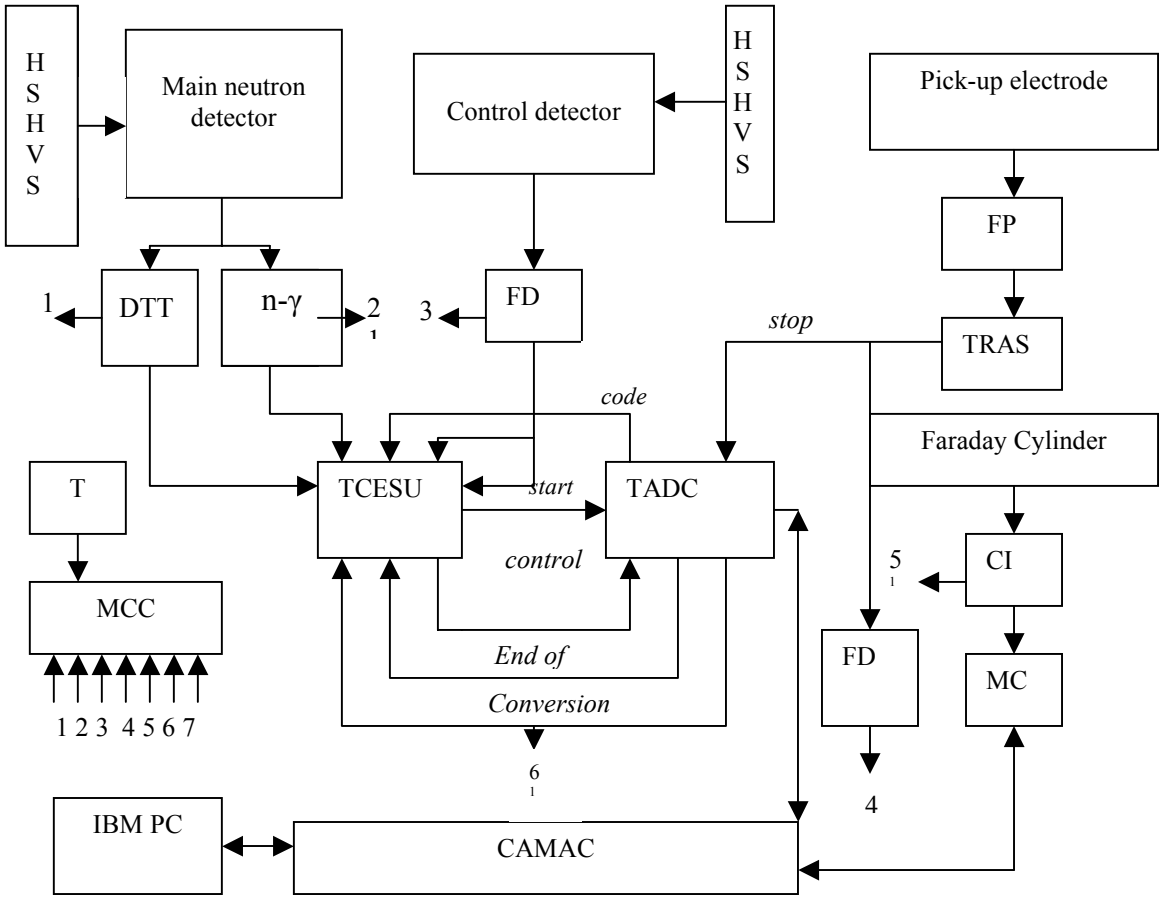

Fig. 2. Block diagram of the system for data recording and accumulation

HSHVS — high-stability high-voltage sources; DTT — discriminator with tracking threshold; n-γ — separation unit, FD — fast discriminator; TADC — time-analog-to-digital converter; TCESU — two-channel event selection unit; FP — fast preamplifier; TRAS — time reference amplifier-shaper; CI — current integrator; MC — monitor counter; FD — frequency divider; T — timer; MCC — multichannel counter.

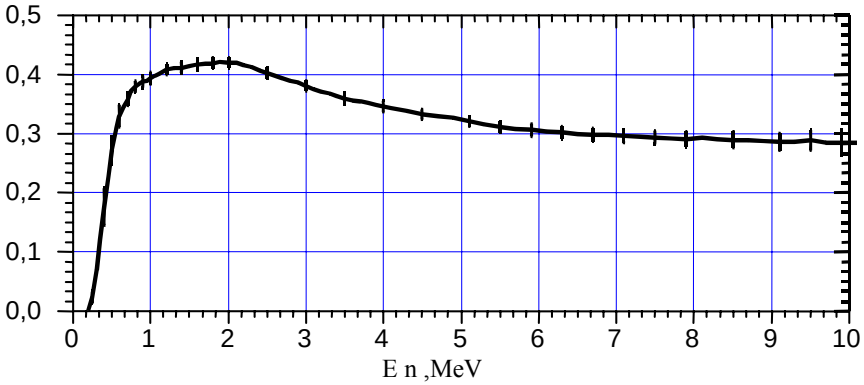

Fig. 3. Neutron detector efficiency

Error determination

Differential neutron emission cross-sections were determined using the following expression:

$$d\sigma(\Theta)/(dE \cdot d\Omega) = N(E,\Theta) \cdot 4\pi/(N_0 \cdot \Omega \cdot n_{nuc} \cdot t \cdot \varepsilon(E_n))$$

where: $N(E,\theta)$) is the number of neutrons of energy E_n registered by the detector at the angle θ;

N_0 is the number of protons striking the target over the measurement time $N(E,\theta)$, $N_0=Q=q \cdot I$ (Q is the number of charges passing through the target; I is the current integrator readings; q is the coefficient for converting the number of charges into the current integrator readings);

θ is the angle at which the detector is positioned relative to the direction of the incident beam;

Ω is the solid angle at which the detector "sees" the target;

$\varepsilon(E_n)$ is the neutron detector efficiency;

n_{nuc} is the number of nuclei in cm^3;

t is the thickness of the target in cm $n_{nuc} \cdot t = h/A \cdot A_{Av,}$ where h is the thickness of the target in g/cm^2, A is the atomic number of the target nucleus and A_{Av} is the Avogadro number.

Attenuation of the neutron flux as a result of scattering on the target holder walls was no more than 0.8% and was not taken into account in the calculations. However, this possible error value was added to the systematic error.

The relative error in determining the differential cross-section was determined using the formula:

$$\delta[d\sigma(\Theta)/(dE_n \cdot d\Omega)] = \sqrt{\delta^2 N(E_n) + \delta^2 N_0 + \delta^2(h) + \delta^2(\varepsilon) + \delta^2(\Omega)} + \delta_{syst}.$$

The relative error in determining N(E) is determined as follows:

$$\delta N(E_n) = \sqrt{\delta^2 N(t) + 9\delta^2 t + 9\delta^2 L_{stat}} + 3\delta L_{syst},$$

where: $\delta N(t)$ is the relative statistical error of the time spectrum;

δt is the relative error in measuring the time of flight;

δL_{stat} is the relative error due to the statistical spread of the point of interaction of the incident particle in the scintillator (0.0088);

δL_{syst} is the relative error due to the measurement accuracy of the time base (0.0044).

δN_0 is the relative error in determining the number of protons striking the target, i.e. (to a high-accuracy of estimation) the number of protons reaching the Faraday cylinder. $\delta N_0 = \delta I + \delta q$, where δI is the relative error in determining the total number of current integrator counts. It consists of a negligibly low statistical error in the number of integrator counts and a random error due to change in the number of background counts (i.e. integrator counts when there is no beam) during the measurement process. The number of current integrator background counts changed periodically at different times of the day and on different days of the week. The measurement data show that the number ranged from 0.01 to 2% of the number of integrator counts at a current of 0.25 μA. This current value corresponded to its averaged value during the experiment. Since the integrator background count value was not determined during the measurement process, the maximum value of the background contribution was also included in the δI determination error as a systematic error. δq is the relative error in determining the relation of the charge delivered by the particles in the beam to the Faraday cylinder and the number of current integrator counts. This relation was determined during the calibration measurements using the stabilized current source. Our resultant evaluated value is δq = 0.007. Thus, the total error in determining the number of protons passing through the target is estimated to be δN_0 = 0.027.

δh is the relative error in the target thickness in the part where the beam passes through. It comprises the error in determining this and the error due to the non-uniformity of the target as regards its thickness. The latter error is due to the uncertainty regarding the place where the beam strikes the target, which can be different each time the beam is applied to the target. Part of the error in determining the target thickness is due to the accuracy of the weighing and measurement of the dimensions of the target foil and is

$$\delta h' = \sqrt{\delta^2 P + 4\delta^2 d} \ ,$$

where δP is the relative weighing error which, on average, is approximately 0.007, and δd is the error in measuring the linear dimensions of the foil, δd = 0.0025. Thus, δh' is 0.0086. The foil thicknesses we measured deviated by no more than 0.4% from the passport data, which fits in completely with the error we adopted. The error due to the non-uniformity of the target thickness can be estimated only approximately based on the difference in the total number of counts in time spectra measured under identical conditions. We estimate that this error does not exceed 2.5%.

$\delta\Omega$ is the relative error in determining the solid angle.

$\delta\varepsilon$ is the relative error in measuring the efficiency. Disregarding the error in determining the number of fragments and the detector aperture diameter, which is compensated by a similar contribution to the $\delta\Omega$ error, we may assume that it comprises the error in measuring the time spectrum of neutrons emitted during fission of ^{252}Cf and in converting this spectrum to an energy spectrum, and the error in measuring the reference spectrum. To this we must add the error due to a possible shift in the energy scale owing to error in determining the energy. The contribution of this error is determined by shifting the efficiency curve to the energy resolution.

Thus, the following expression was used to determine the relative error:

$$\delta[d^2\sigma(\Theta)/(dE_n \cdot d\Omega)] = \sqrt{\delta^2 N(t) + 9\delta^2 t + \delta^2(\varepsilon) + 0.0169} + 0.0126 \, .$$

When determining the error of angle-integrated spectra

$$d\sigma(E_n)/dE_n = \iint d\sigma(E,\Theta)/(dE_n \cdot d\Omega) \cdot d\Theta \cdot d\Omega \ ,$$

the systematic errors and errors in determining the efficiency were deducted from the total error of the double-differential spectra, the contribution from statistical errors to the error in determining the integral spectrum was determined, and then the systematic error and the error in determining the efficiency were added back.

Table 1 gives the individual components and the total relative errors for the differential and integral neutron spectra obtained for scattering of protons with an energy of approximately 9 MeV, using their calculation for ^{124}Sn as an example.

Table 1

E_n	$\delta N(t)$	δt	$\delta\varepsilon$	δL	δh	$\delta\Omega$	δ_{syst}	δ_{diff}	δ_{integ}
0.3	0.019	0.007	0.464	0.013	0.025	0.008	0.0086	0.475	0.199
0.5	0.012	0.009	0.086	0.013	0.025	0.008	0.0086	0.108	0.049
0.7	0.0007	0.011	0.032	0.013	0.025	0.008	0.0086	0.071	0.034
1.0	0.0004	0.013	0.0246	0.013	0.025	0.008	0.0086	0.071	0.034
2.0	0.0003	0.018	0.0214	0.013	0.025	0.008	0.0086	0.081	0.038
3.0	0.0003	0.021	0.0224	0.013	0.025	0.008	0.0086	0.090	0.042
4.0	0.0006	0.025	0.0273	0.013	0.025	0.008	0.0086	0.100	0.046
6.0	0.0020	0.030	0.0353	0.013	0.025	0.008	0.0086	0.117	0.053
8.0	0.036	0.036	0.0475	0.013	0.025	0.008	0.0086	0.157	0.061
10.0	0.051	0.039	0.0629	0.013	0.025	0.008	0.0086	0.145	0.070

Error in determining the neutron energy

The error in determining the neutron energy was calculated using the formula

$$\delta E = 2\sqrt{\delta^2 t + \delta^2 L_{stat}} + \delta L_{syst},$$

where δt, δL_{stat} and δL_{syst} are similar to the relative errors in determining the time of flight and the time base when calculating the error in determining the cross-sections. The spread in the initial energy of the energy particles caused by the slowing down of protons in the material being studied must be added to the E_n error given in the Table.

Table 2

Absolute energy scale errors

E_n, MeV	0.3	0.5	0.7	1.0	2.0	3.0	4.0	6.0	8.0	10.0
ΔEn, MeV	0.007	0.012	0.018	0.027	0.060	0.098	0.141	0.238	0.346	0.469

Energy calibration of the accelerator

To determine the energy of the protons in the beam, energy calibration of the accelerator was carried out. The energy of the accelerated particles (protons) was determined from the kinematic correlations between its and the energy of secondary particles [11–12] emitted by the nuclei of elements with a well-defined level structure. The ^{27}Al(p,n)^{27}Si and ^{56}Fe(p,n)^{56}Co reactions were used in this study. Calibration measurements were performed for practically every change in proton energy. Then, using the entire set of data obtained for all energies, the method of least squares was used to find the functional dependence in the form: y = ax + b, where x = «f^2» and f is the frequency of the nuclear magnetic resonance at which the proton

beam appears on the target and a and b are the parameters. For the EGP-15 accelerator, E_p = 0.75596+0.06337f^2 (MeV), if «f» is in MHz, and for the EGP-10M accelerator E_p = 0.25744+0.0162$(f-1.018)^2$ (MeV).

Experiment

The measurements were performed in the following sequence: the specified proton energy was set, the detector was positioned for the selected scattering angle and the element to be studied was put in position by successive remote switching of the foils. One position in the six-position target holder was used to measure the background and the calibration foil (made of Al) was installed in another. If one of the elements to be studied had a clearly defined level structure itself (e.g. ^{56}Fe), the additional calibration foil was not installed. The measurements at one angle started and finished with background measurements. The measurement time at each position depended on the average beam current but was set in the calculation at no more than half an hour. We then proceeded to the next angle, etc. After all the angles had been measured, a new series of similar measurements was performed. When the necessary count statistics had been gathered, another proton energy was set and the measurements repeated. After going from the minimum to the maximum energy, the measurements were again repeated with the energy moving in the reverse direction. If the results coincided we could be sure that the accelerator control systems were operating reliably. Measurements were carried out on two similar spectrometers. The first was based on the EGP-10M accelerator, the second on the EGP-15. On the first spectrometer, measurements were carried out at proton energies of 6.94, 8.11, 8.73, 9.165 and 9.59 MeV, and on the second at 10.24, 10.77 and 11.20 MeV. However, on the latter measurements were also performed at energies close to the proton energies on the first accelerator, namely 8.11, 8.79 and 9.18 MeV. Figure 4 shows spectra of neutrons scattered on samples made of ^{116}Sn at an initial energy of E_p = 8.11 MeV obtained on the different accelerators with foils of different thickness. There was clearly a high level of agreement between the data from both experiments carried out ten months apart.

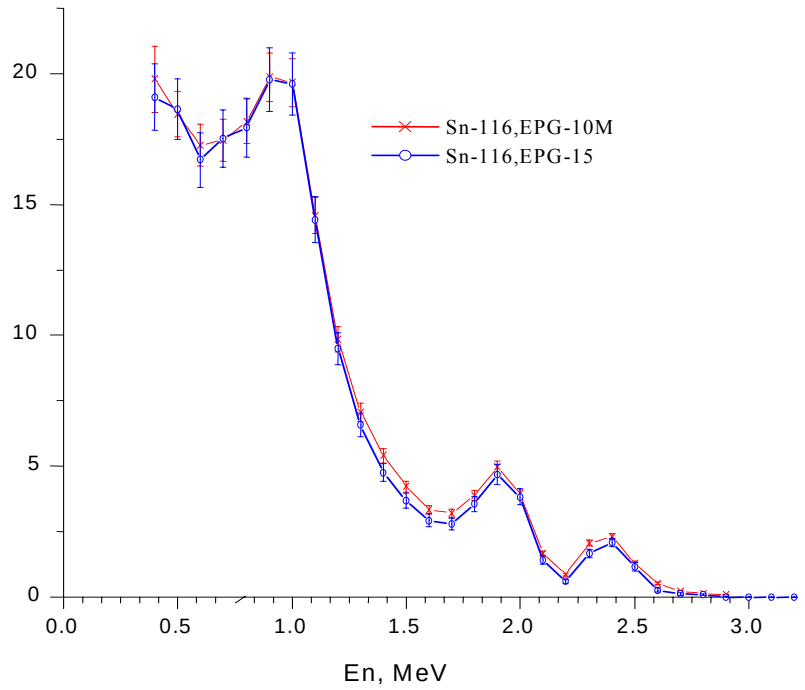

Fig. 4. Comparison of the results of experiments carried out on the EPG-10M accelerator (x) and on the EGP-15 (o) accelerator.

Results of the experiment

We obtained cross-sections differential in neutron emission angle and energy and cross-sections differential in neutron energy for the (p,n) reaction on the above-mentioned isotopes of tin, lead and bismuth at incident proton energies of 10.24, 10.77 and 11.19 MeV. The results of the experiment in the laboratory system of coordinates are shown in Figs 5–25. Cross-sections differential in neutron energy at proton energies of 6.94, 8.11, 8.73, 9.16 and 9.59 MeV were obtained by multiplying the spectra measured for the angle of 105º by 4π. Since EXFOR contains no data on the angular and energy distributions for the isotopes studied here, the total cross-sections were compared with those given in Refs [1–5]. Since the cross-sections obtained here are limited to a neutron energy range starting at 0.4 MeV, extrapolation to zero energy was performed. For this, cross-sections differential in energy were calculated using the level density parameters and models giving the best description of the spectra obtained by us [13]. The calculated spectra and experimental spectra were stitched together and, in the neutron energy region below 0.4 MeV the calculated data were used to obtain the total cross-sections. When integrating the differential spectra, the contribution of the error in introducing the calculated part of the spectrum was assumed to be equal to the proportion of the calculated part of the spectrum in the total spectrum. For the purposes of comparison with the data in Ref. [1], integration of the spectra was carried out for the neutron energy range starting at 1 MeV. Figures 5 and 25 compare the data obtained in this way with the data of other authors. The data obtained by us agree well with the data in Ref. [2] obtained for lower proton energies, and satisfactorily with the data in Ref. [1]; however, they differ rather markedly from the data in Ref. [3] for ^{118}Sn and ^{124}Sn, and from the data in Ref. [4] for Bi.

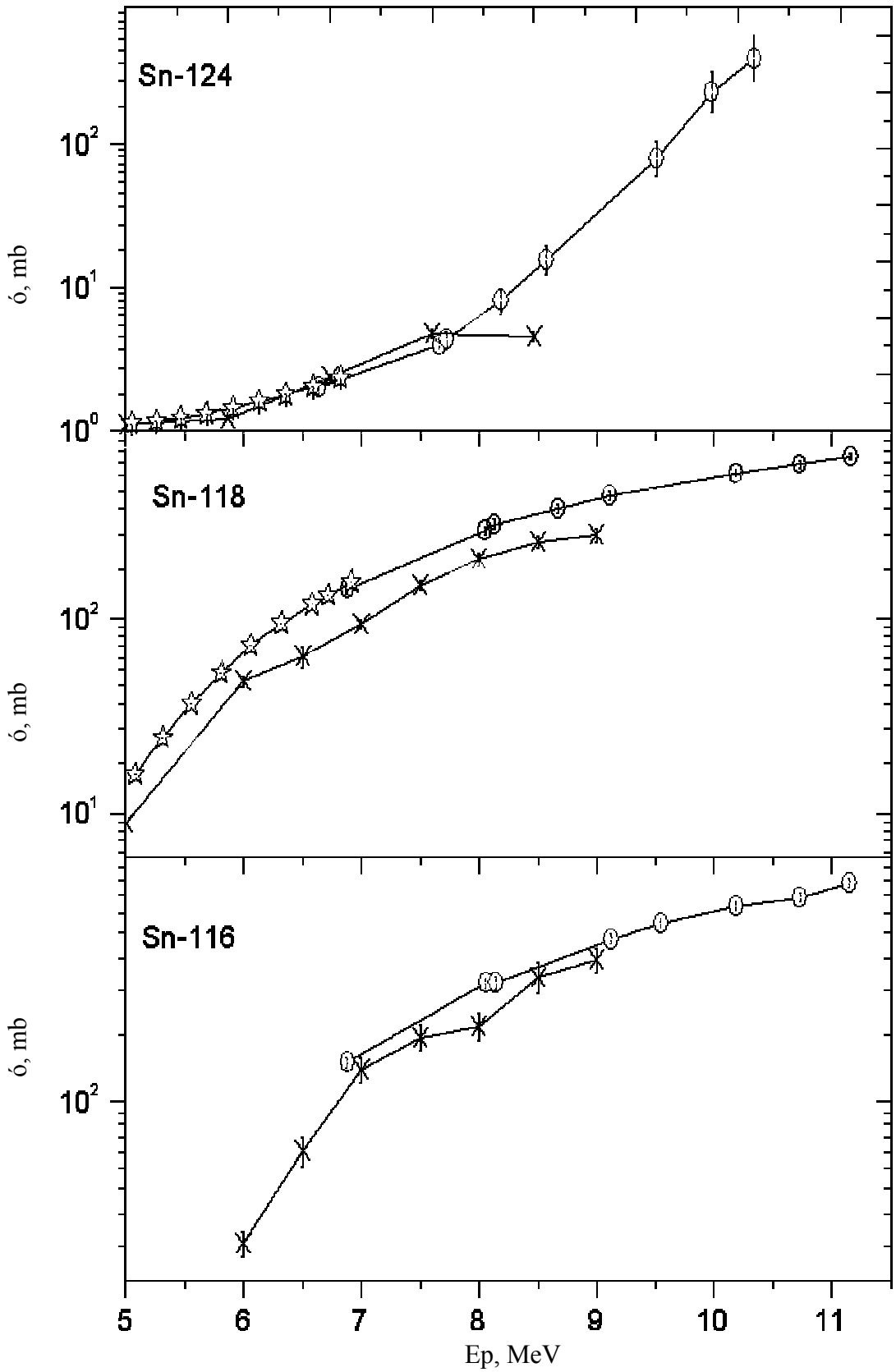

Fig. 5. Total cross-sections obtained from the experiments carried out by us (o), and in Ref. [2] (☆) and Ref. [3] (×).

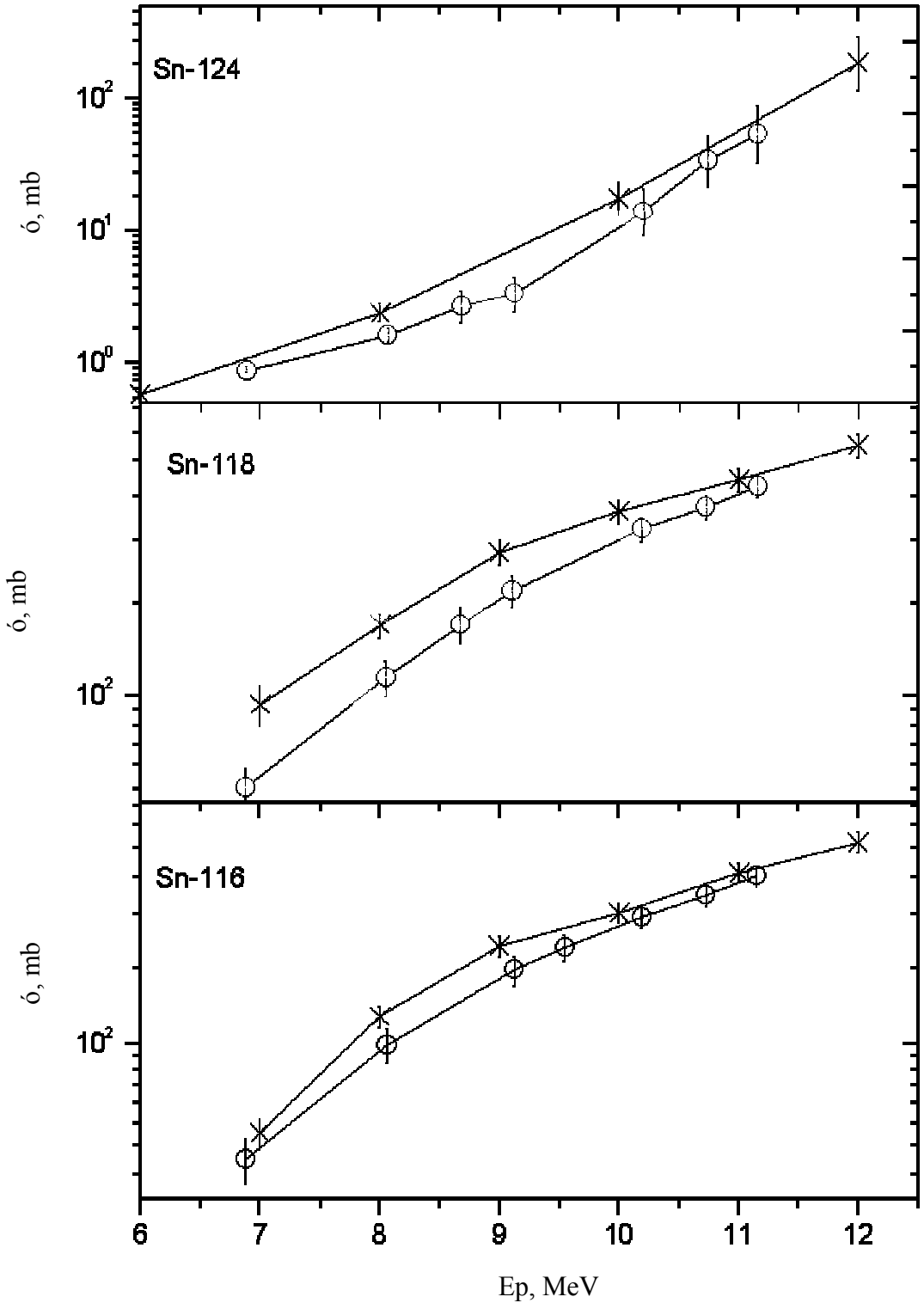

Fig. 6. Cross-sections obtained by integrating the differential spectra from a neutron energy of 1 MeV: this paper – o, Ref. [1] – ×.

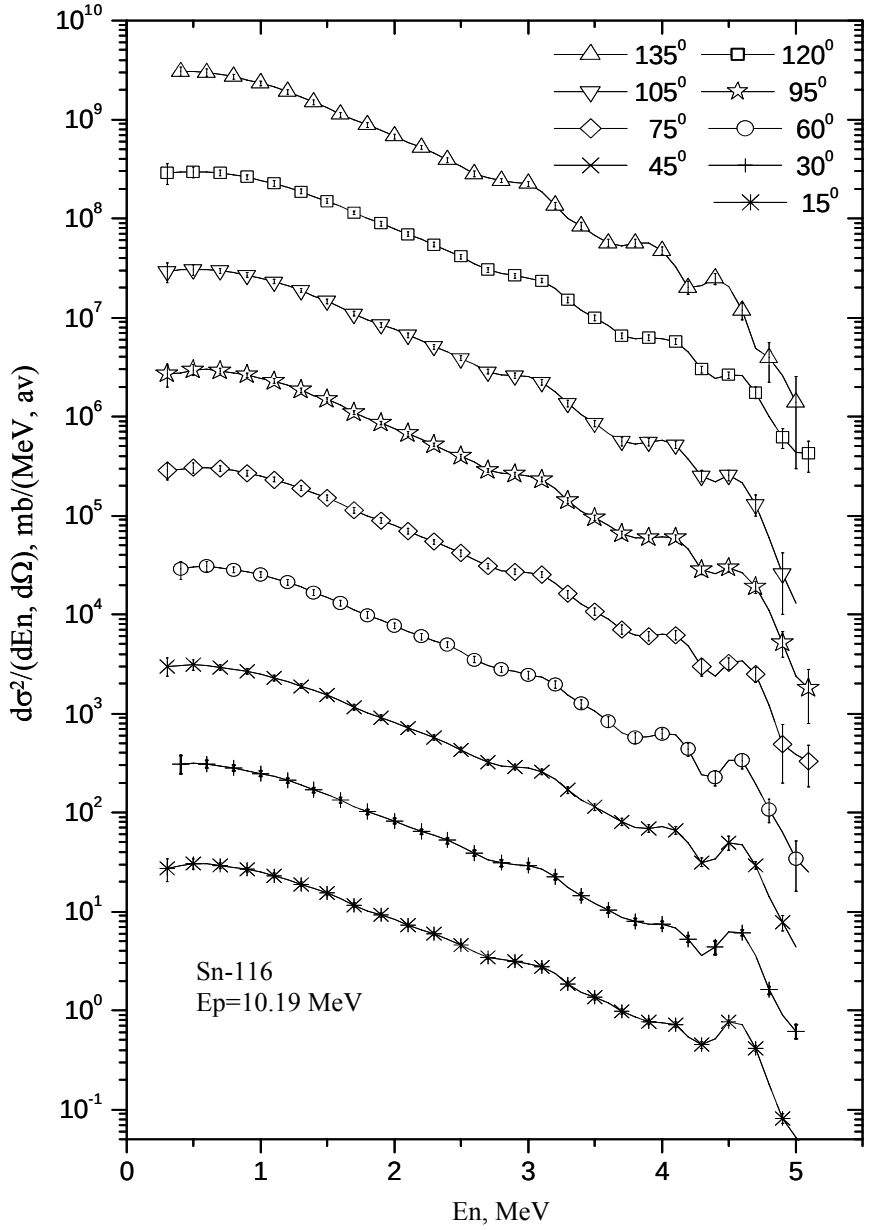

Fig. 7. Double differential cross-sections for the ^{116}Sn(p,n) reaction at an average proton beam energy of 10.19 MeV. The values for the scattering angles 30º, 45º, 60º, 75º, 95º, 105º,120º and 140º are exaggerated by 1, 2, 3, 4, 5, 6, 7 and 8 orders of magnitude respectively.

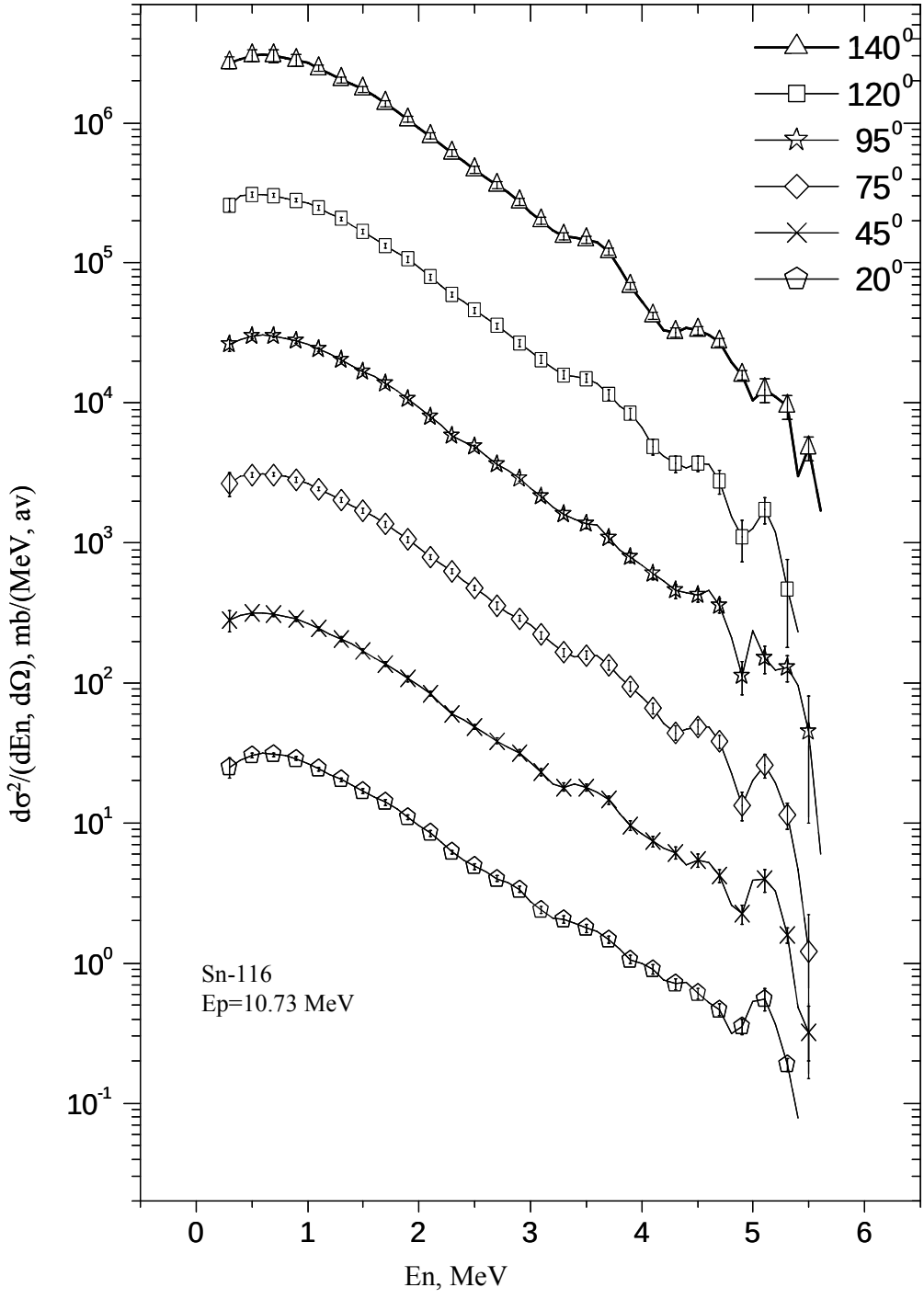

Fig. 8. Double differential cross-sections for the ^{116}Sn(p,n) reaction at an average proton beam energy of 10.73 MeV. The values for the scattering angles 45º, 75º, 95º,120º and 140º are exaggerated by 1, 2, 3, 4 and 5 orders of magnitude respectively.

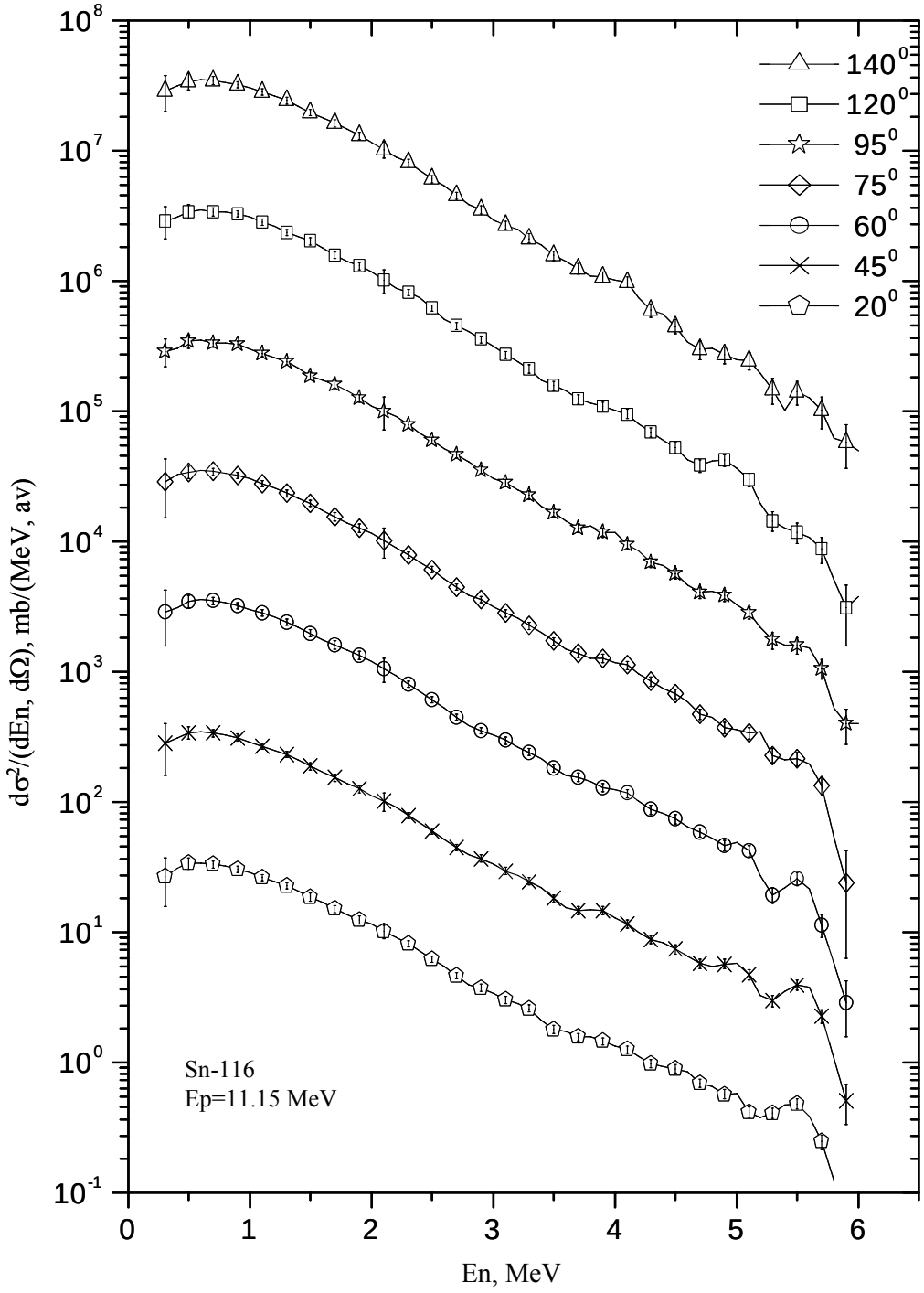

Fig. 9. Double differential cross-sections for the ^{116}Sn(p,n) reaction at an average proton beam energy of 11.15 MeV. The values for the scattering angles 45º, 60º, 75º, 95º,120º and 140º are exaggerated by 1, 2, 3, 4, 5 and 6 orders of magnitude respectively.

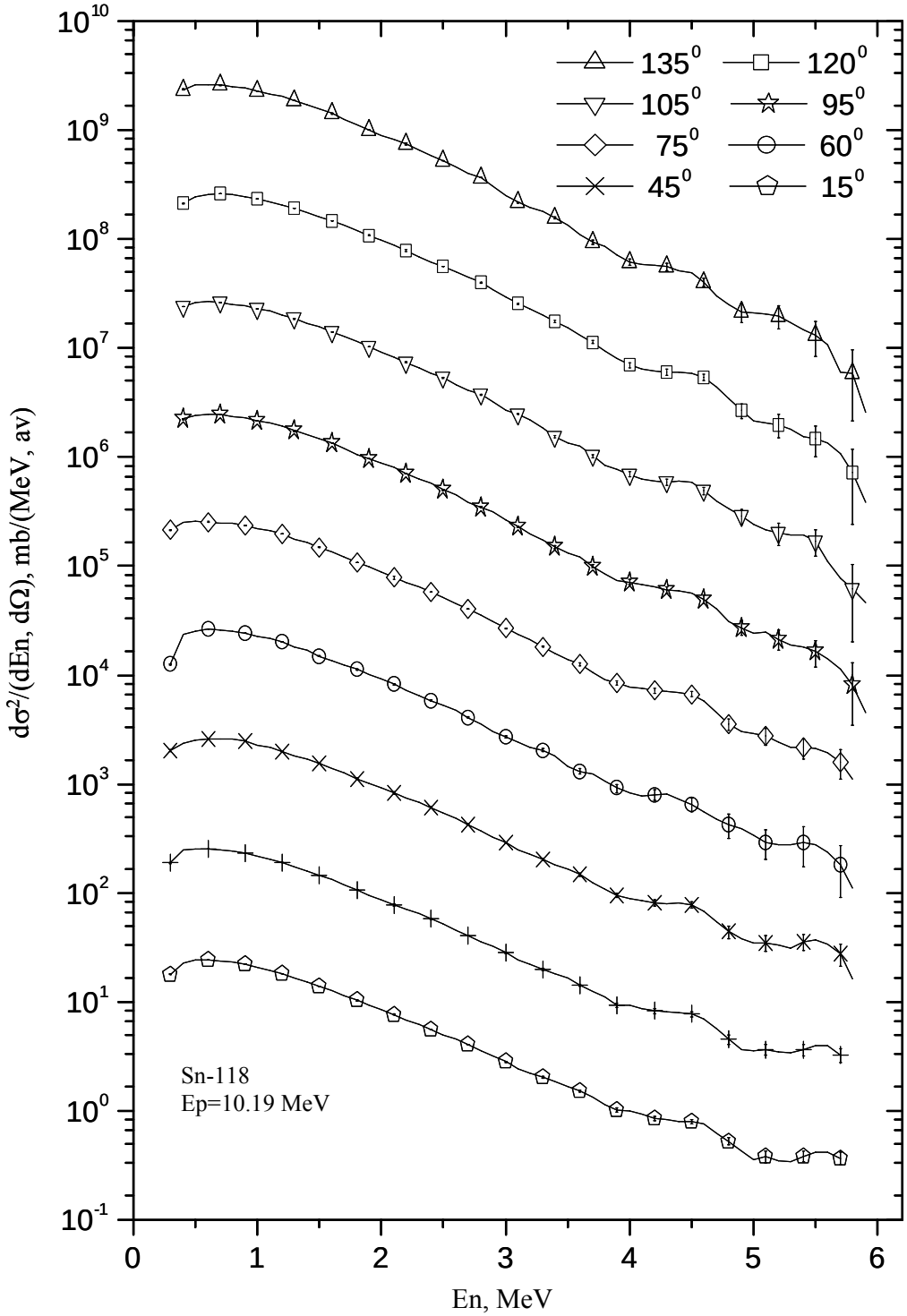

Fig. 10. Double differential cross-sections for the ^{118}Sn(p,n) reaction at an average proton beam energy of 10.19 MeV. The values for the scattering angles 30º, 45º, 60º, 75º, 95º, 105º,120º and 140º are exaggerated by 1, 2, 3, 4, 5, 6, 7 and 8 orders of magnitude respectively.

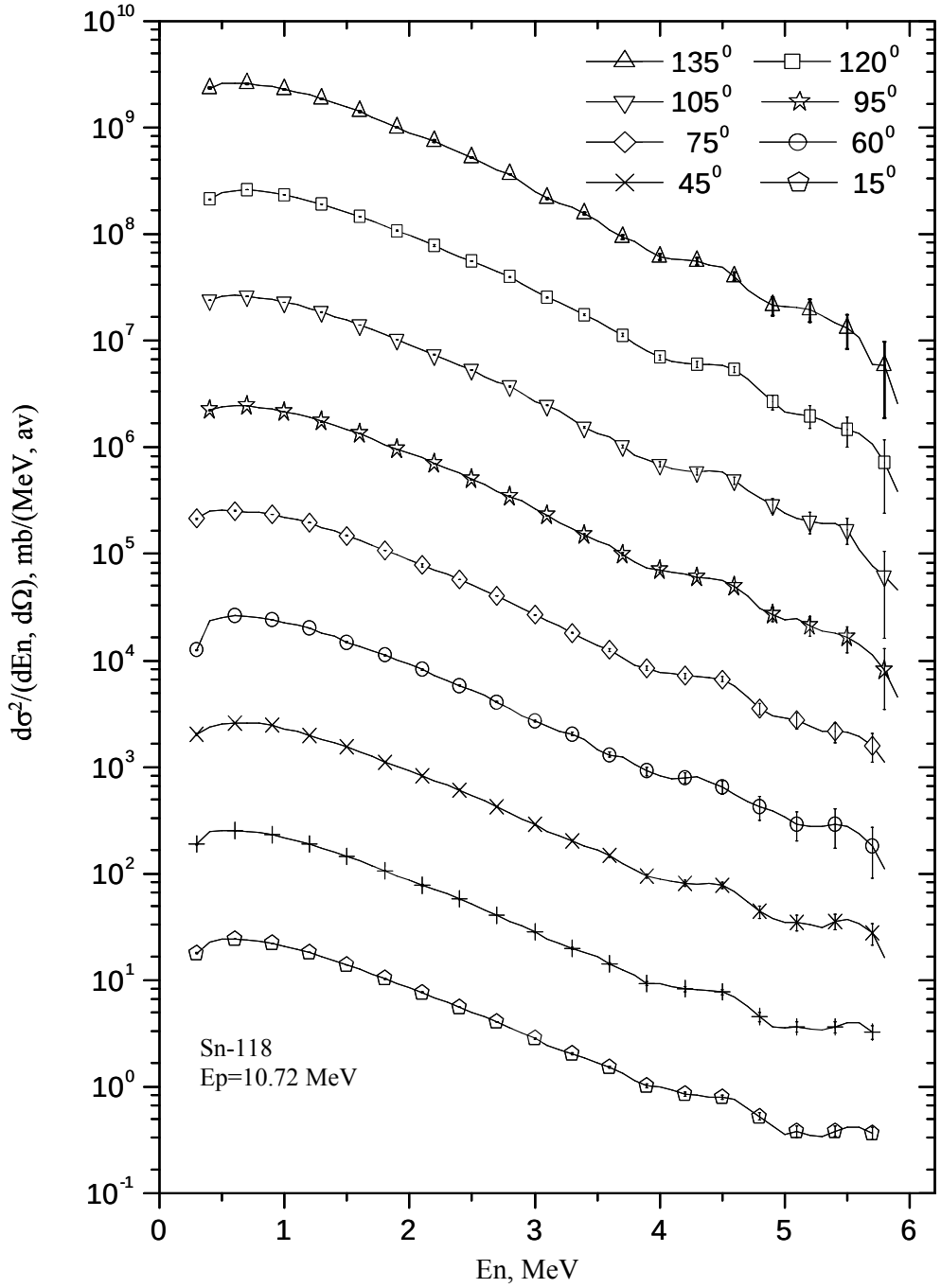

Fig. 11. Double differential cross-sections for the ^{118}Sn reaction at an average proton beam energy of 10.72 MeV. The values for the scattering angles 45º, 60º, 75º, 95º,120º and 135º are exaggerated by 1, 2, 3, 4, 5 and 6 orders of magnitude respectively.

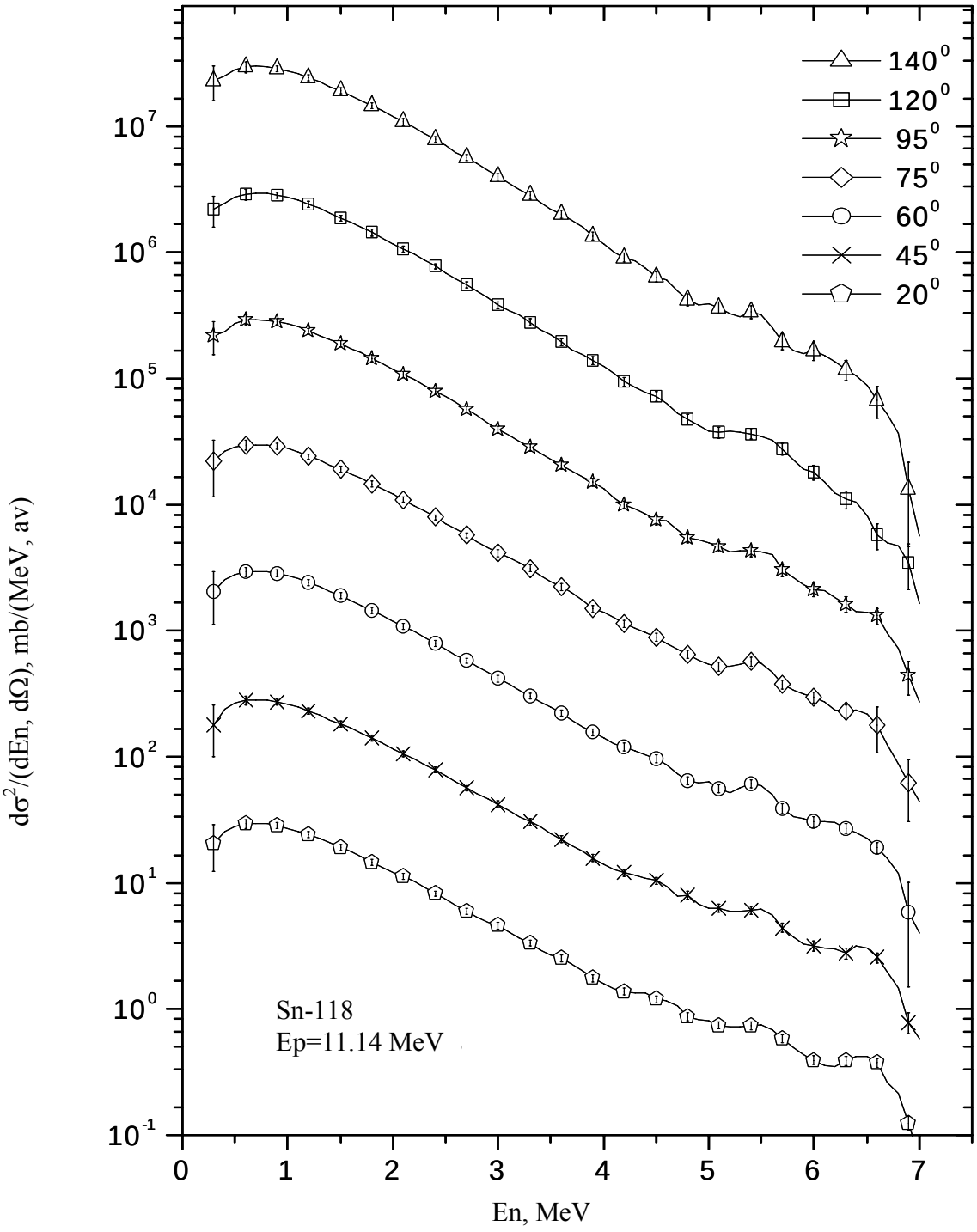

Fig. 12. Double differential cross-sections for the ^{118}Sn(p,n) reaction at an average proton beam energy of 11.14 MeV. The values for the scattering angles 45º, 60º, 75º, 95º,120º and 140º are exaggerated by 1, 2, 3, 4, 5 and 6 orders of magnitude respectively.

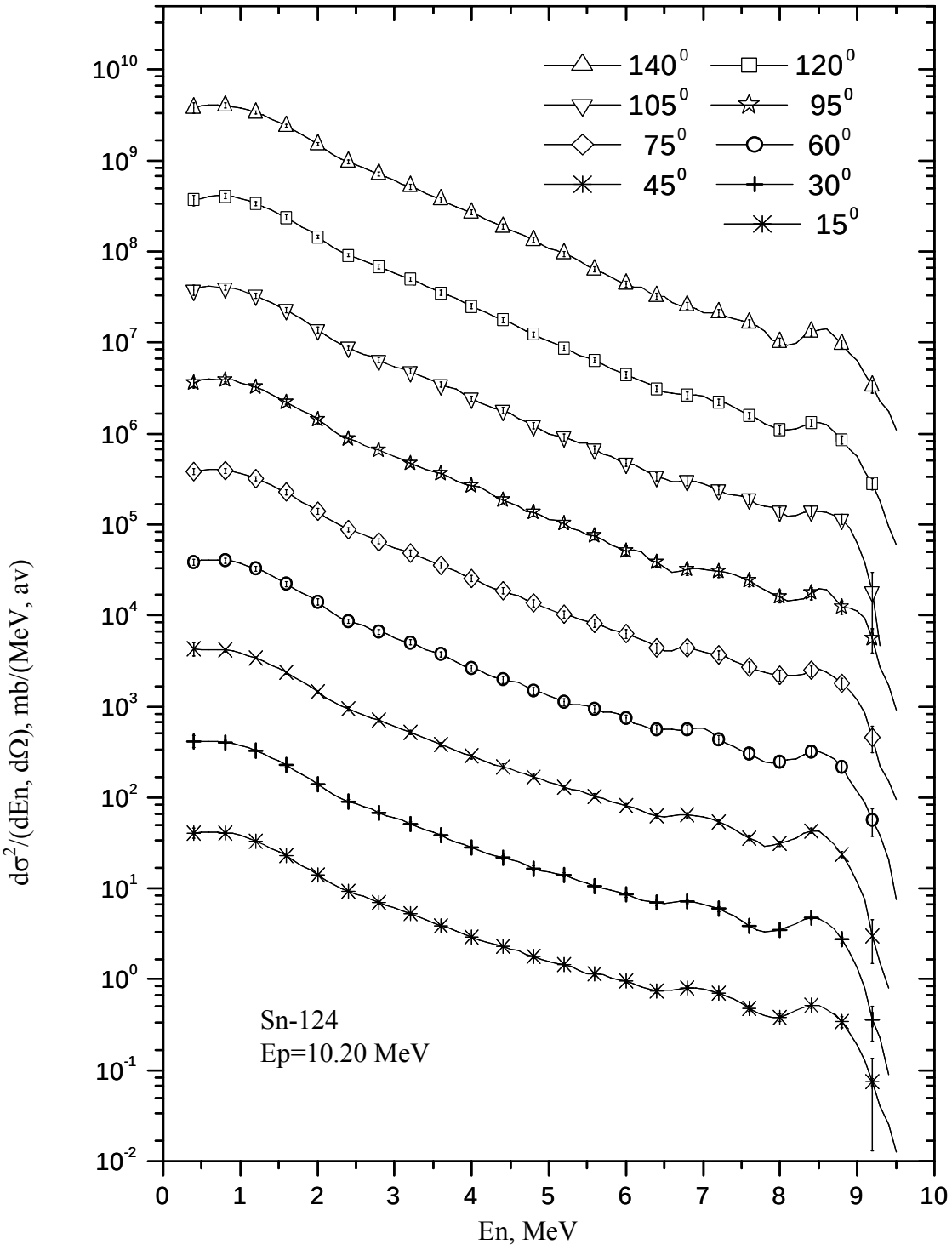

Fig. 13. Double differential cross-sections for the ^{124}Sn(p,n) reaction at an average proton beam energy of 10.20 MeV. The values for the scattering angles 30º, 45º, 60º, 75º, 95º, 105º,120º and 140º are exaggerated by 1, 2, 3, 4, 5, 6, 7 and 8 orders of magnitude respectively.

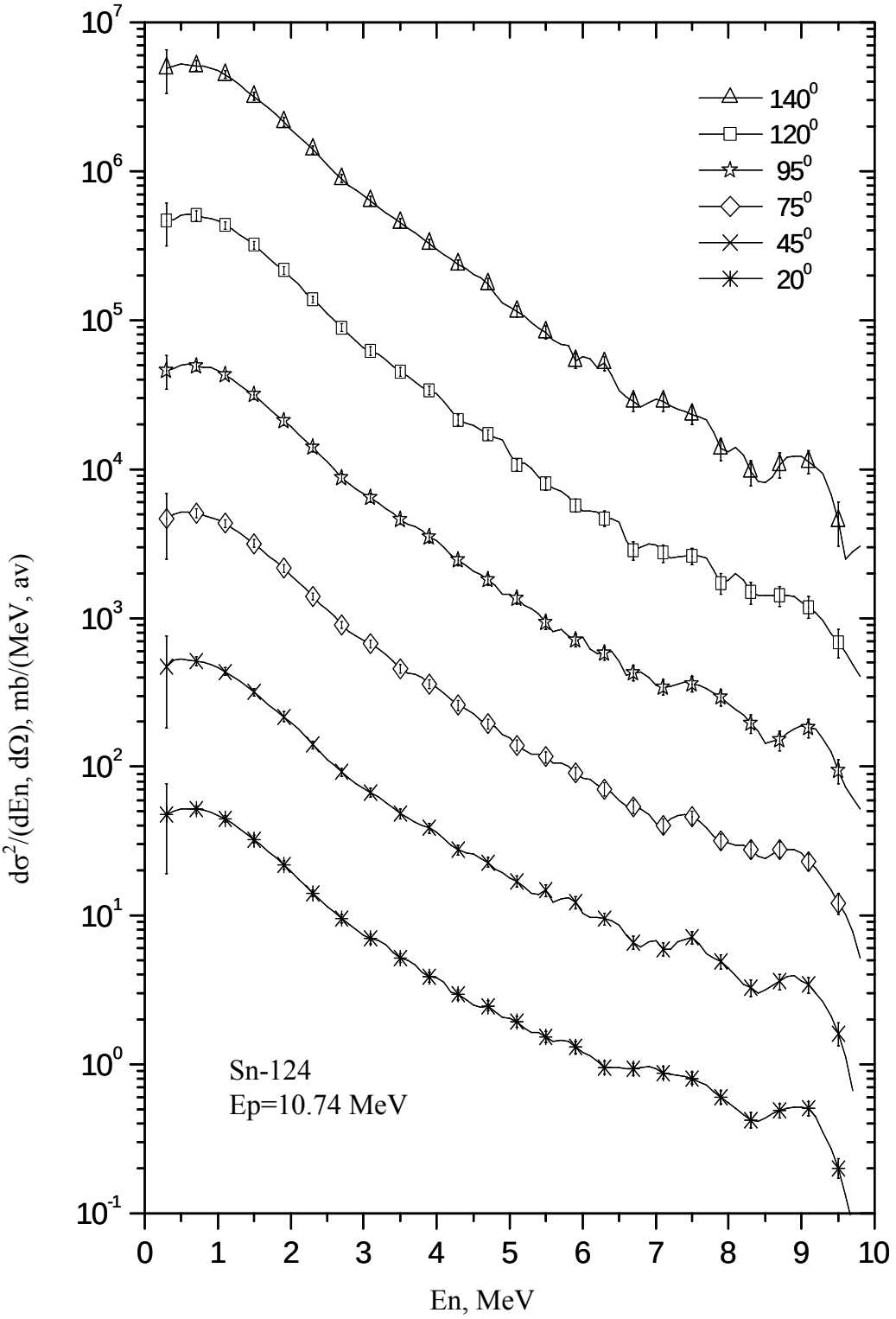

Fig. 14. Double differential cross-sections for the ^{124}Sn(p,n) reaction at an average proton beam energy of 10.74 MeV. The values for the scattering angles 45º, 75º, 95º,120º and 140º are exaggerated by 1, 2, 3, 4 and 5 orders of magnitude respectively.

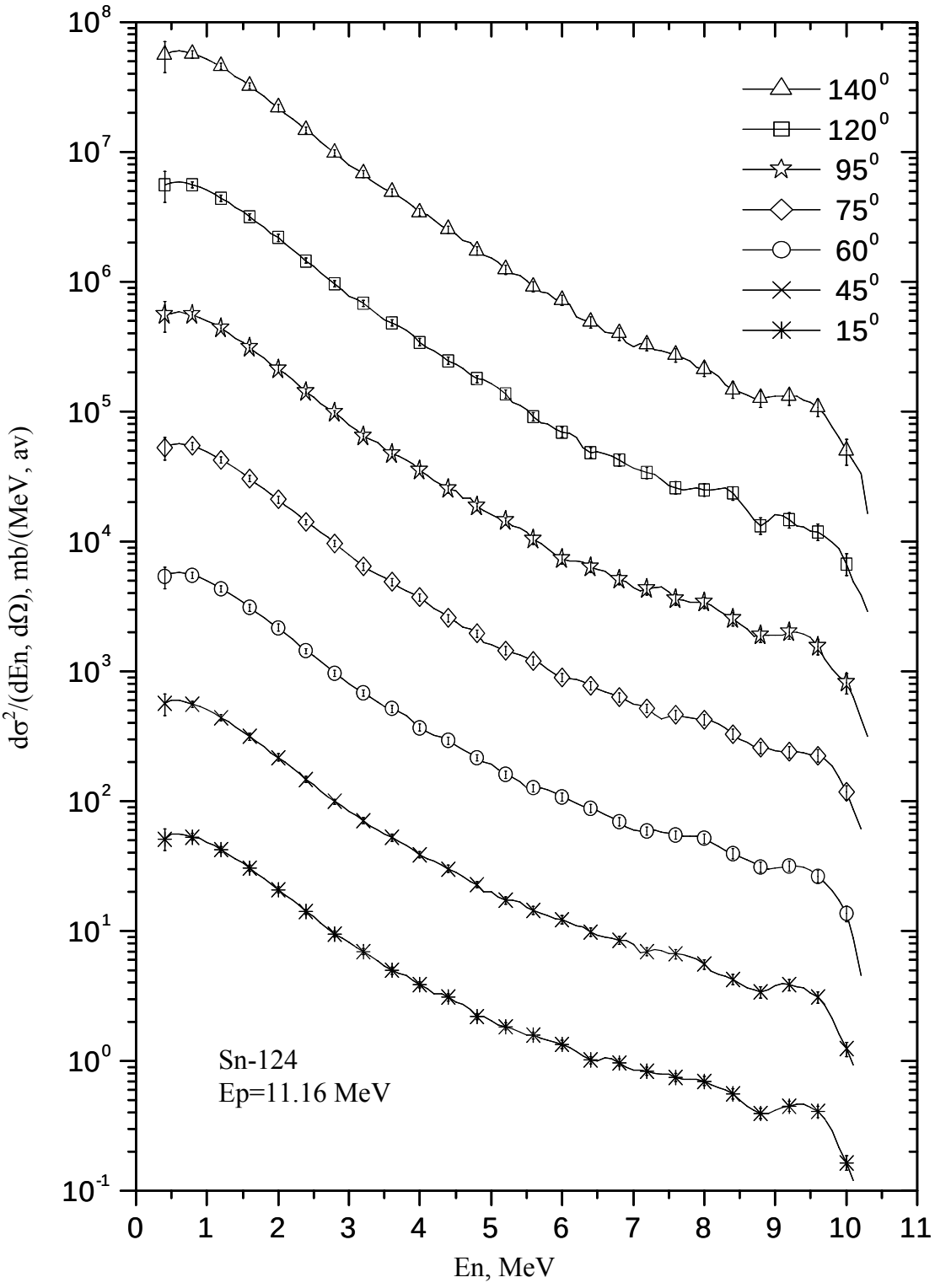

Fig. 15. Double differential cross-sections for the ^{124}Sn(p,n) reaction at an average proton beam energy of 11.16 MeV. The values for the scattering angles 45º, 60º, 75º, 95º,120º and 140º are exaggerated by 1, 2, 3, 4, 5 and 6 orders of magnitude respectively.

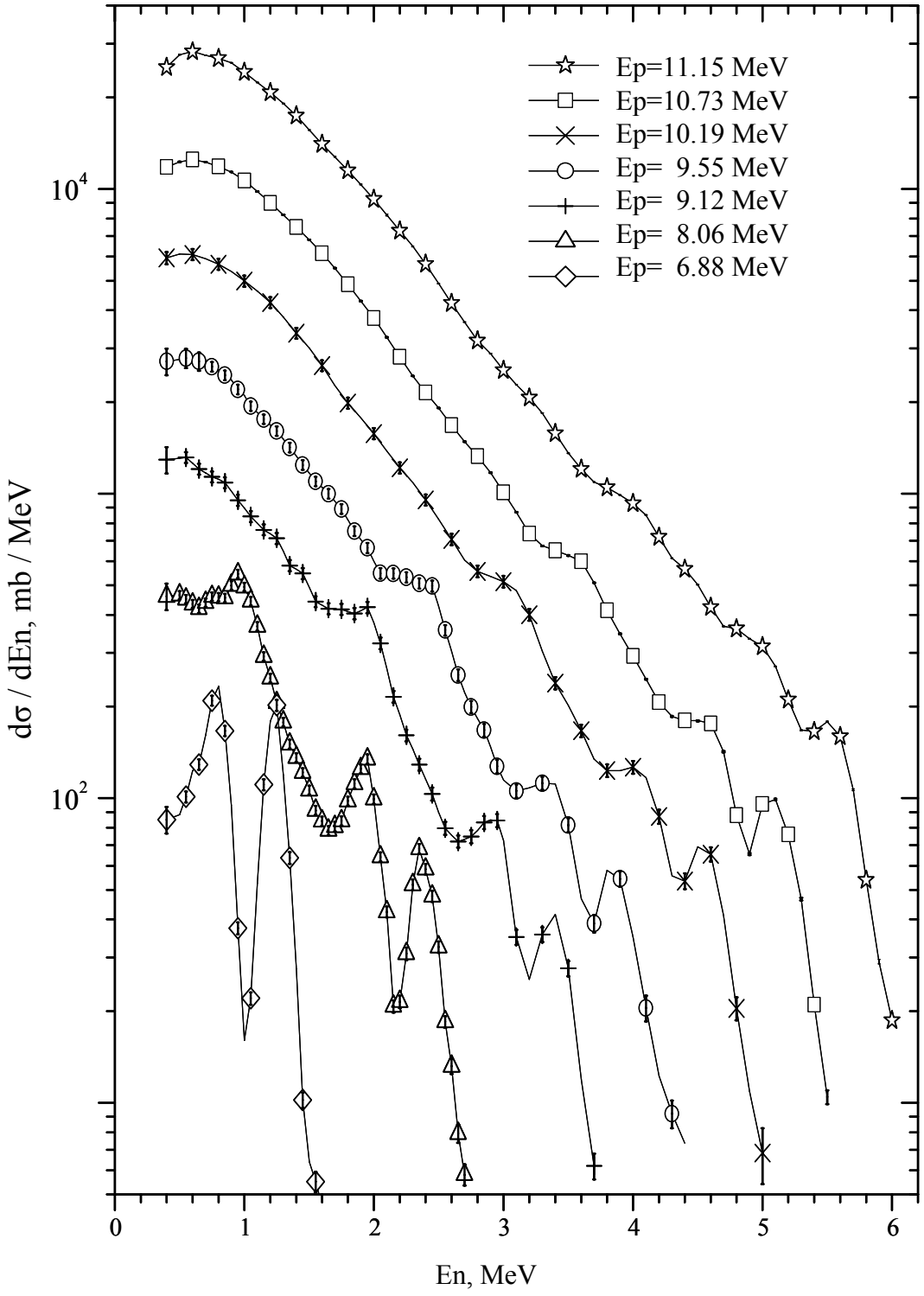

Fig. 16. Integral neutron spectra from the reaction $^{116}Sn(p,n)^{116}Sb$. The values at <Ep> = 11.15, 10.73, 10.19, 9.55, 9.12 and 8.06 MeV are multiplied by 64, 32, 16, 8, 4 and 2 respectively

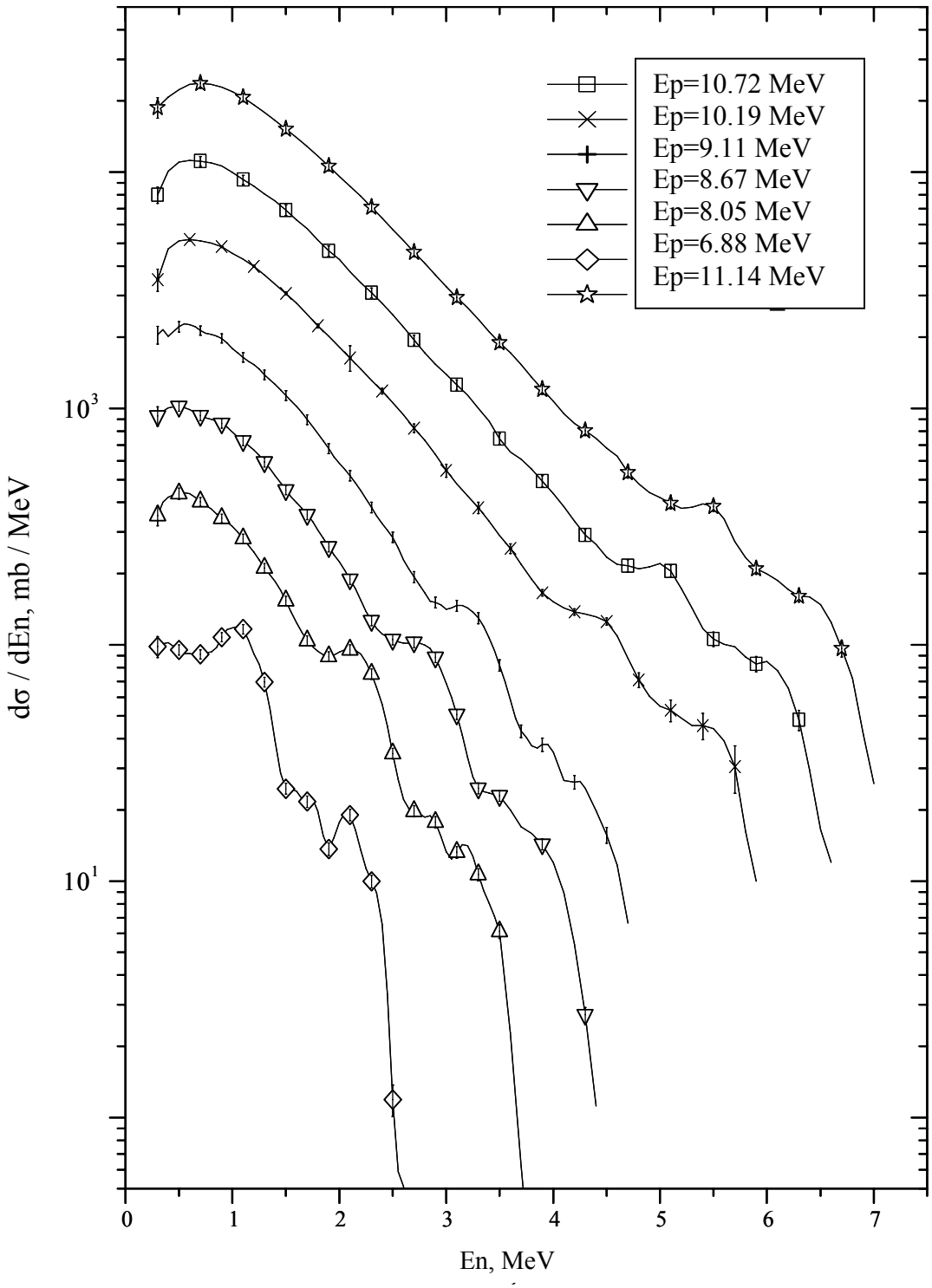

Fig. 17. Integral neutron spectra from the reaction $^{118}Sn(p,n)^{118}Sb$. The values at <Ep> = 11.14, 10.72, 10.19, 9.11, 8.67 and 8.05 MeV are multiplied by 64, 32, 16, 8, 4 and 2 respectively

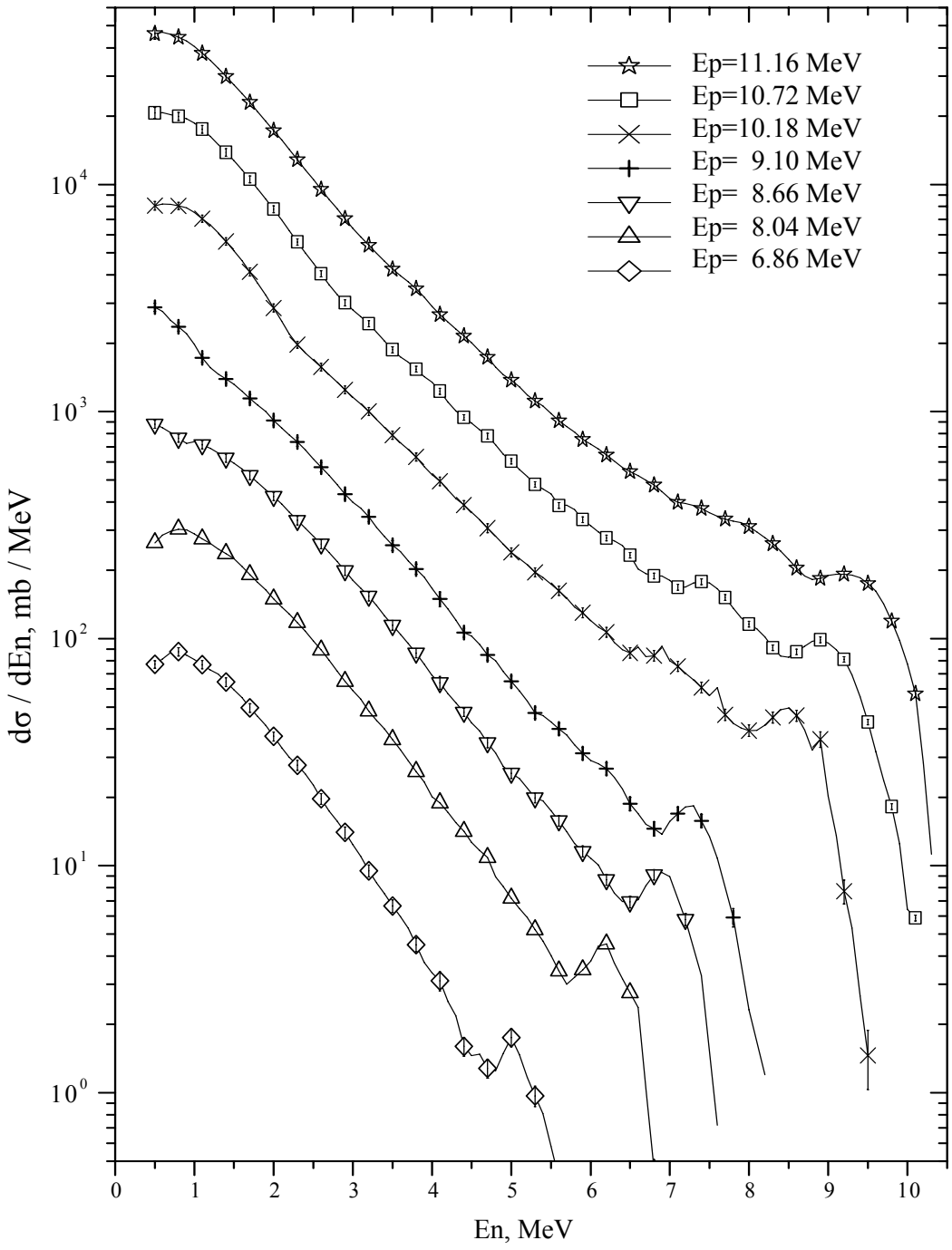

Fig. 18. Integral neutron spectra from the reaction $^{124}Sn(p,n)^{124}Sb$. The values at <Ep> = 11.16, 10.72, 10.18, 9.10, 8.66 and 8.04 are multiplied by 64, 32, 16, 8, 4 and 2 respectively.

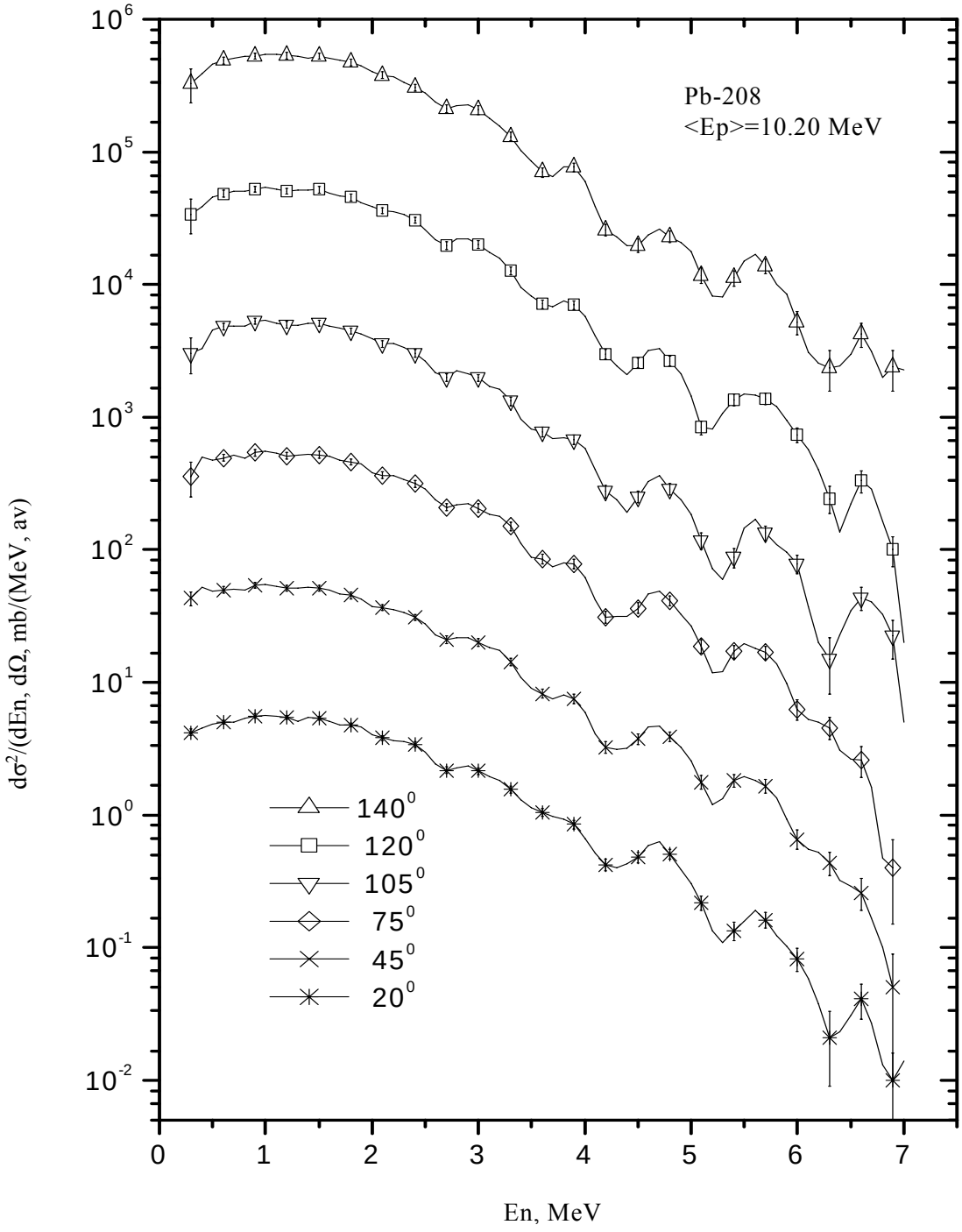

Fig. 19. Double differential cross-sections for the ^{208}Pb(p,n)^{208}Bi reaction at an average proton beam energy of 10.20 MeV. The values for the scattering angles 45º, 75º, 105º,120º and 140º are exaggerated by 1, 2, 3, 4 and 5 orders of magnitude respectively.

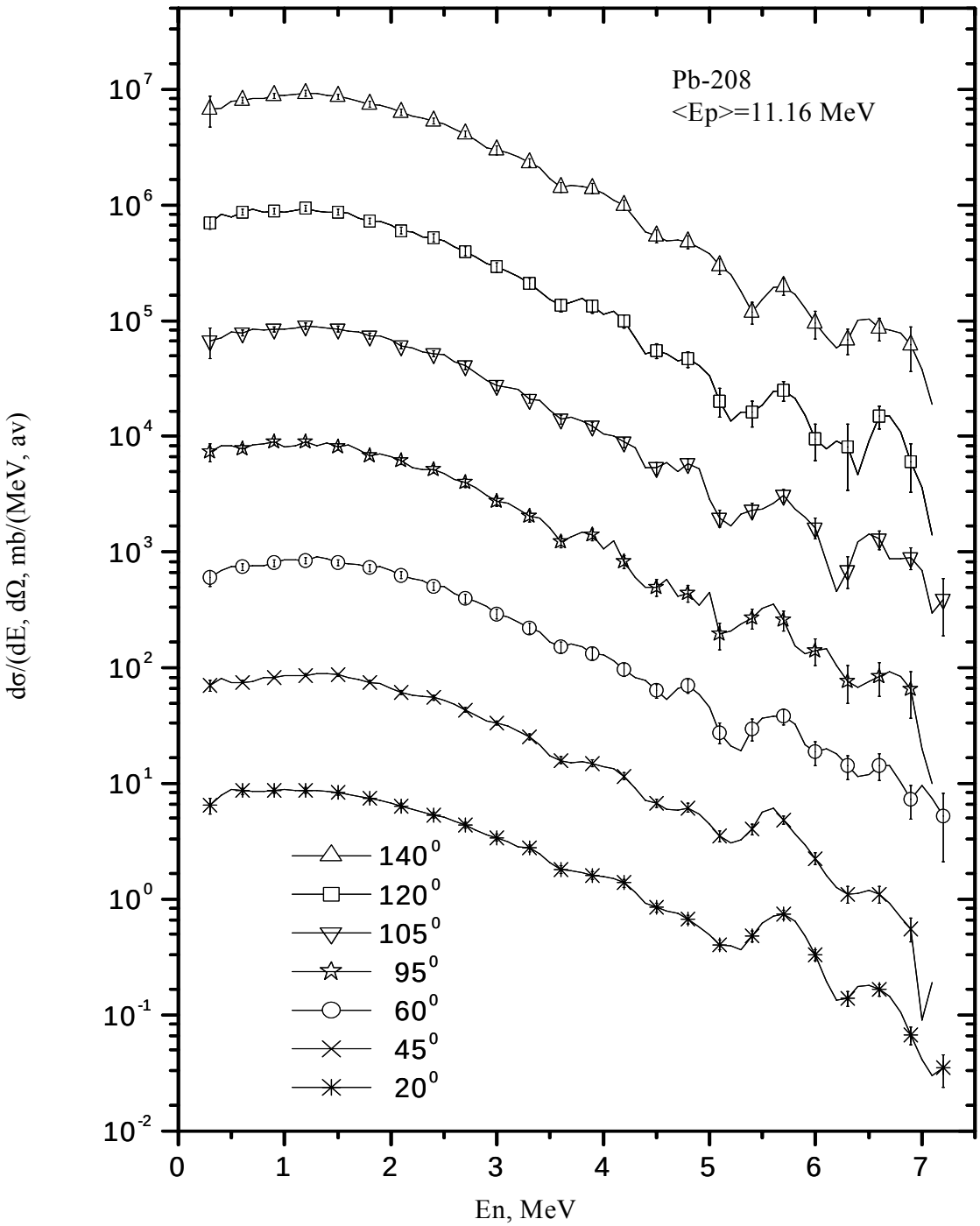

Fig. 20. Double differential cross-sections for the ^{208}Pb(p,n)^{208}Bi reaction at an average proton beam energy of 11.16 MeV. The values for the scattering angles 45º, 60º, 95º,105º, 120º and 140º are exaggerated by 1, 2, 3, 4, 5 and 6 orders of magnitude respectively.

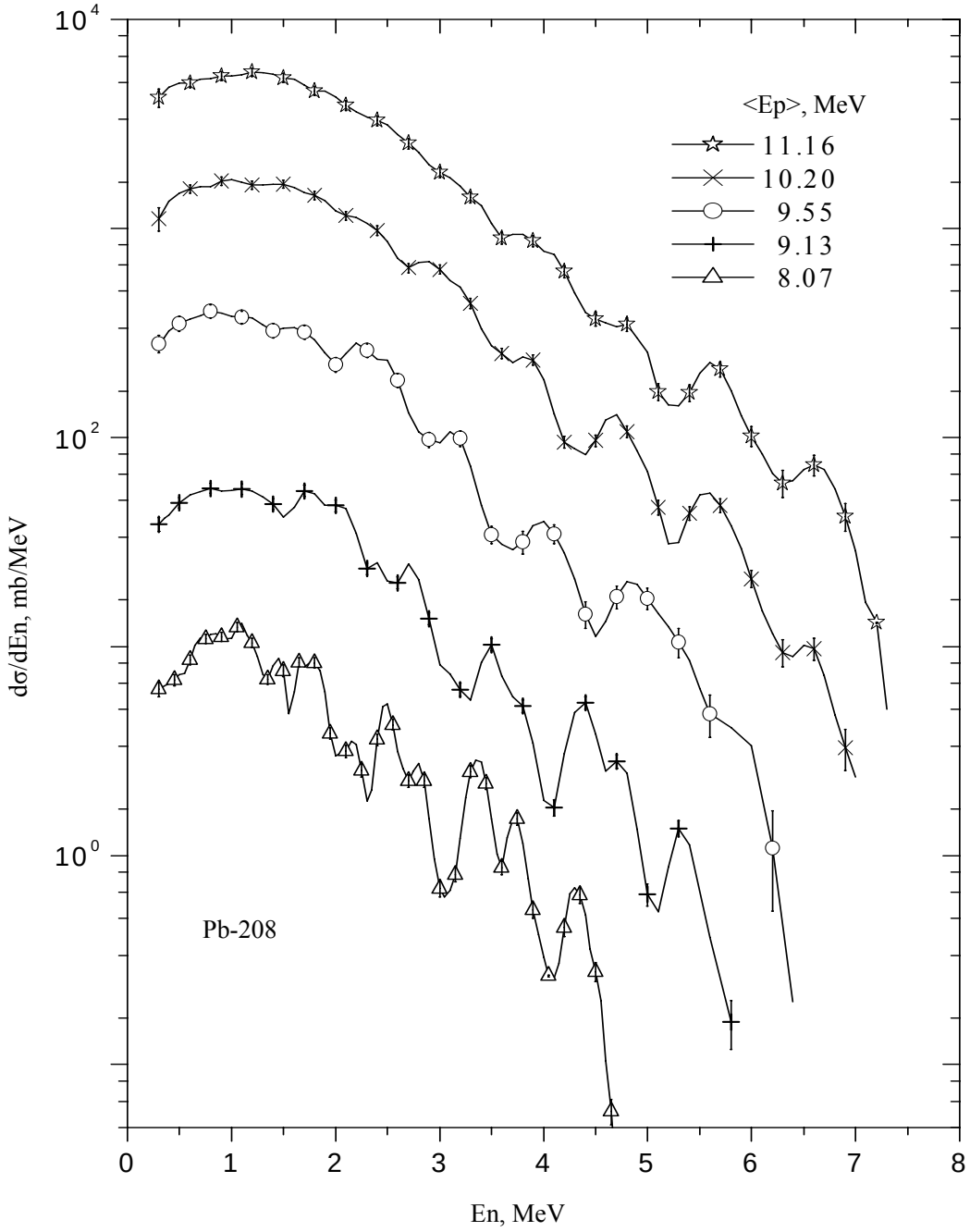

Fig. 21. Integral neutron spectra from the reaction ^{208}Pb (p,n)^{208}Bi. The values for <Ep> = 9.55, 10.20 and 11.16 MeV are multiplied by 10, 25 and 50 respectively

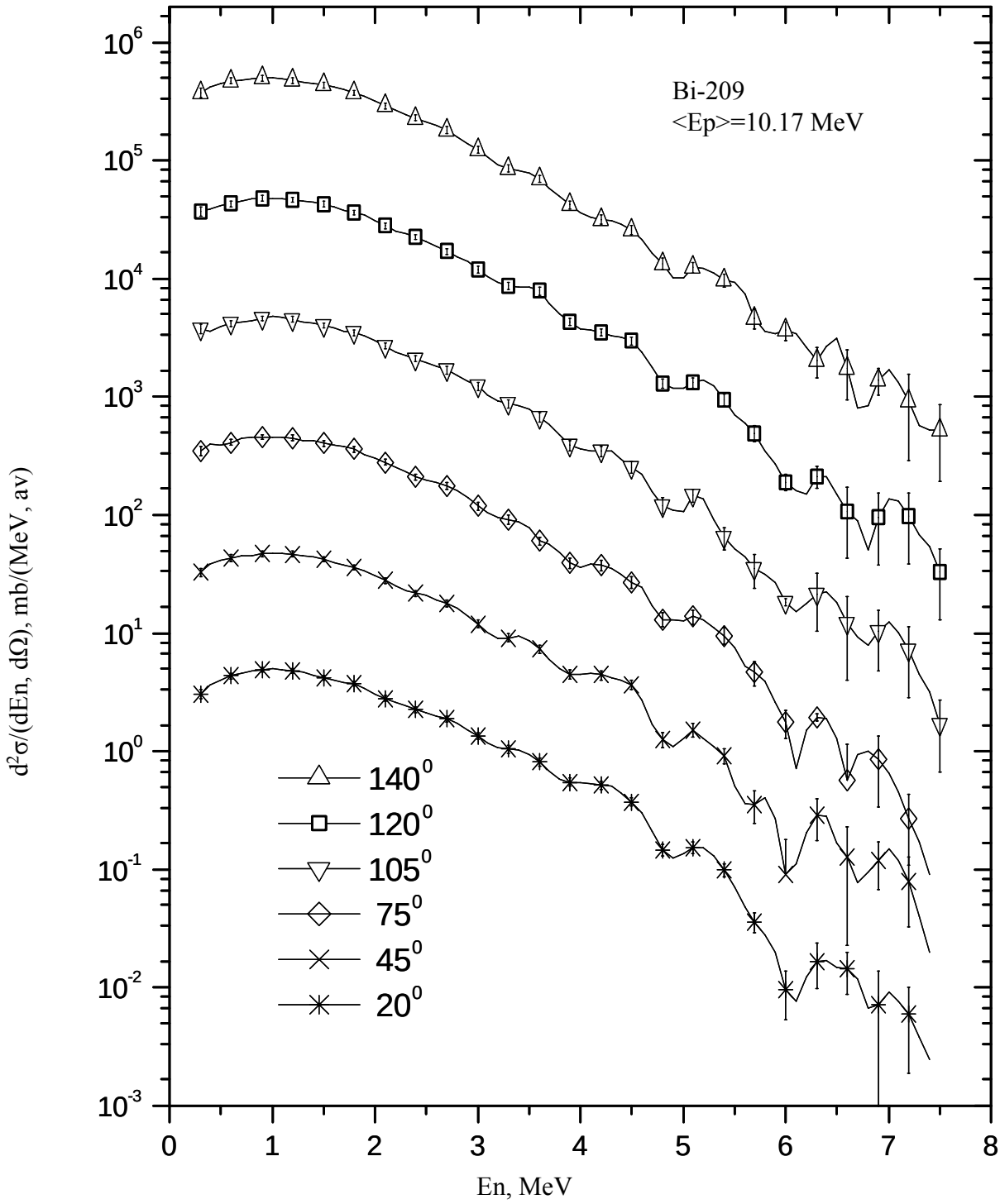

Fig. 22. Double differential cross-sections for the ^{209}Bi(p,n) reaction at an average proton beam energy of 10.17 MeV. The values for the scattering angles 45º, 75º,120º and 140º are exaggerated by 1, 2, 3, 4 and 5 orders of magnitude respectively.

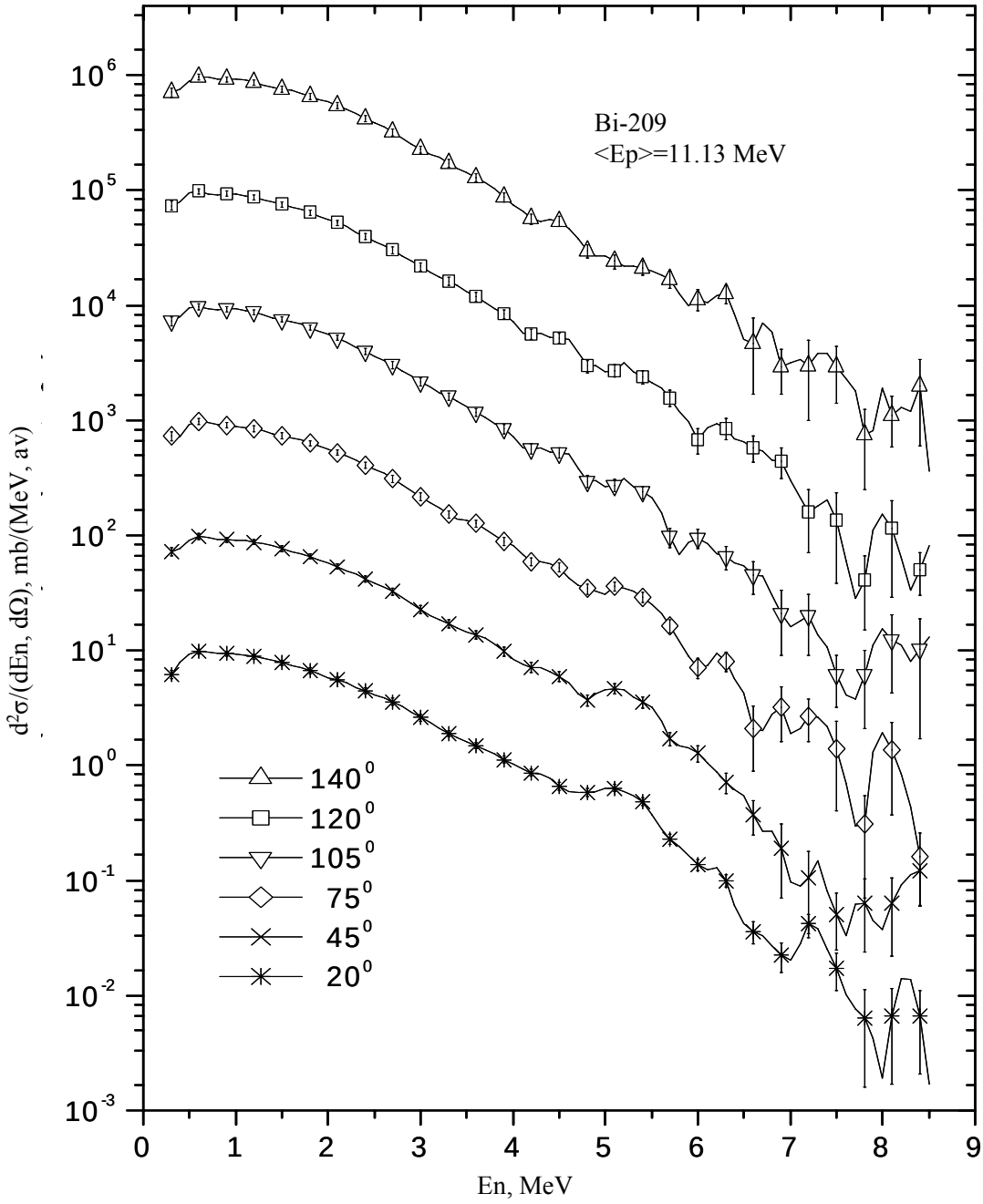

Fig. 23. Double differential cross-sections for the ^{209}Bi(p,n)^{209}Po reaction at an average proton beam energy of 11.13 MeV. The values for the scattering angles 45º, 75º, 105º, 120º and 140º are exaggerated by 1, 2, 3, 4 and 5 orders of magnitude respectively.

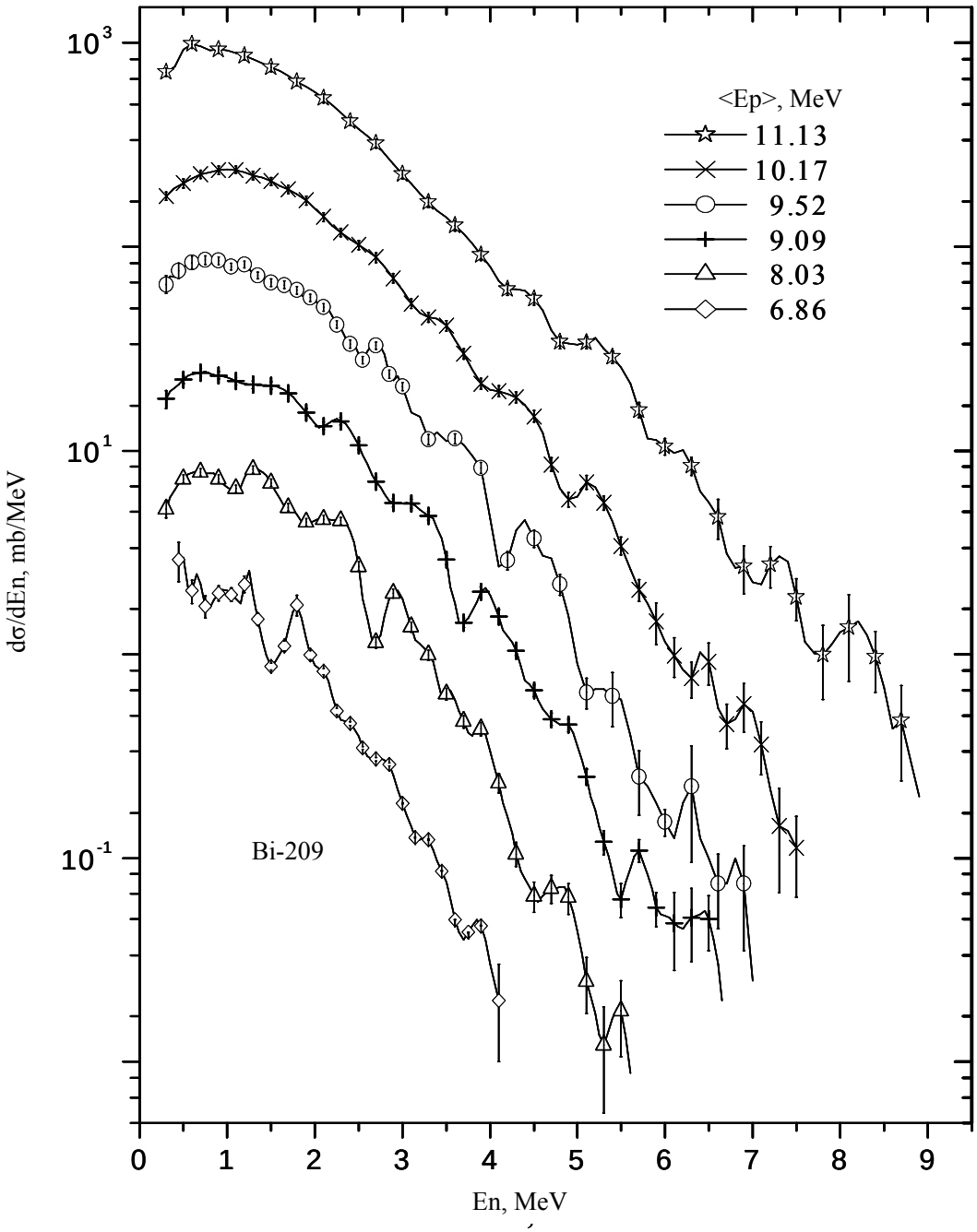

Fig. 24. Integral neutron spectra from the reaction ^{208}Pb (p,n)^{208}Bi. The values for <Ep> = 9.55, 10.20 and 11.16 MeV are multiplied by 10, 25 and 50 respectively.

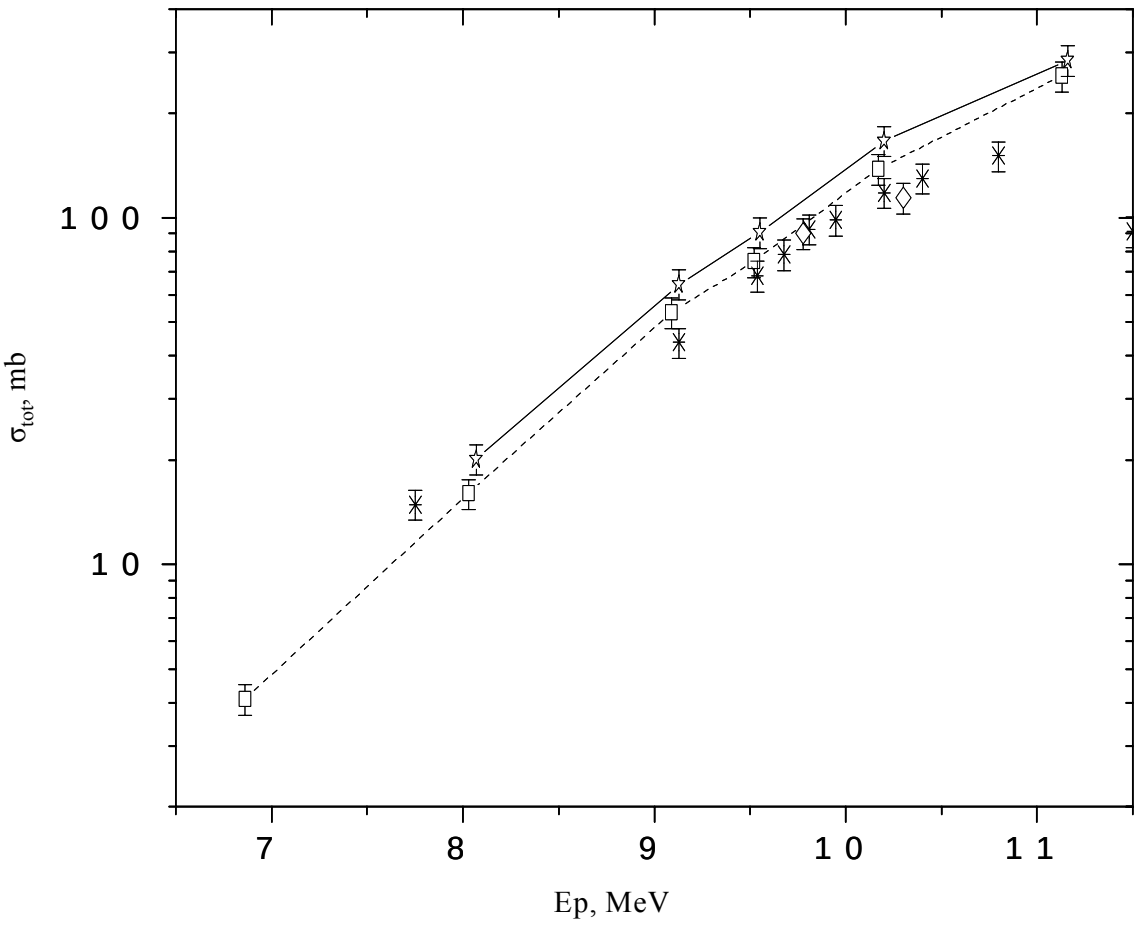

Fig. 25. Total cross-sections obtained from the experiments carried out by us: Bi - □ , Pb - ☆, Bi in Ref [4] – ✳, Ref [5] – ◊.

REFERENCES

1. Wood, R.M., Borchers, R.R. and Barschall, Nucl. Phys., v. 71, No. 3, 1965, pp 529–545.
2. Johnson, C.H., Blair, J.K., et al, Phys. Rev., C 15, 196, 1970.
3. Batij, V.G., Skakun, E.A., C 91, Minsk, 248, 1991.
4. Miyano, K., et al., JPJ, 1978, v. 45, p. 1071.
5. Wing, J., Huizenga, J.R., P.R., 1962, v. 128, p. 280.
6. Andre, C.G., et. al., P.R., 1956, v. 101, p. 645.
7. Demenkov, V.G., Zhuravlev, B.V., Lychagin, A.A., Mil'shin, V.I., Trykova, V.I., Pribory I tekhnika instrumenta, 1995, v. 38, No. 3, pp 314–318 [in Russian].
8. Demenkov, V.G., Zhuravlev, B.V., Lychagin, A.A., PTEh, 1995, v. 38, No. 6, Part 1, pp 738–740 [in Russian].
9. Demenkov, V.G., Zhuravlev, B.V., Lychagin, A.A., Trykova, V.I., Pribori I Tekhnika Ehksperimenta, 2000, No. 2, pp 66–69, [in Russian].
10. Manhart, W., Proc. of Adv. Gr. Meeting, IAEA-TECDOC-410, 1987, Vienna.
11. Baryshnikov, A.I., Abramov, A.I., inventor's certificate No. 317969, [in Russian].
12. Kornilov, N.V., Proc. of Adv. Gr. Meeting, IAEA-TECDOC-410, 1987, Vienna.
13. Zhuravlev, B.V., Lychagin, A.A., Titarenko, N.N., et.al., ISINN-10, May 22–25, 2002, Dubna, JINR, Book of Abstracts, E3-2002-67, p. 72.

04-34911 (211) [2]
Translated from Russian

UDC 539.163

EVALUATION OF THE ^{244}Cm RESOLVED RESONANCE REGION

G.B. Morogovskij, L.A. Bakhanovich
Sosny Joint Institute for Energy and Nuclear Research, Belarus National Academy of Sciences

EVALUATION OF THE ^{244}Cm RESOLVED RESONANCE REGION. Thermal cross-sections, Breit-Wigner parameters and background cross-sections for the representation of the $\sigma_t(E)$, $\sigma_\gamma(E)$ and $\sigma_f(E)$ energy dependence in the 10^{-5}–1000 eV region were obtained by evaluating the resonance integrals and experimental cross-sections at E=0.0253 eV and in the resolved resonance region.

The need for a fairly accurate knowledge of the energy dependence of the radiative capture and fission cross-sections of ^{244}Cm (a strong alpha emitter with a half-life of around 18 years and, consequently, an intensive source of heat to which almost 50% of the heat release in spent fuel after a three-year cooling period can be attributed) is dictated by reprocessing and transport requirements. Moreover, since ^{244}Cm is often an appreciable impurity in samples used to measure the cross-sections of americium and other isotopes of curium, its contribution to the cross-sections being measured needs to be accurately taken into account.

Comparing the existing evaluated nuclear data files ENDF/B-VI, JENDL-3.2, JEF-2 and Ref. [1] in the ^{244}Cm resolved resonance region of interest to us, we can see that the mean resonance parameters and thermal cross-sections calculated using the above evaluations differ significantly, though the evaluations themselves are based on almost exactly the same experimental data (only the ENDF/B-VI and JEF-2 evaluations do not use the measurements from Ref. [2] carried out later). The differences in the resonance integrals of these evaluations also lie mainly in the resolved resonance region (chiefly in the 0.5–10 eV range, i.e. in the 7.67 eV resonance region).The aim of this paper is to produce a set of Breit-Wigner resonance parameters that adequately reproduce the measured resonance integrals and all existing experimental cross-sections in the resolved resonance region.

As in the JENDL-3.2 and JEF-2 evaluations, we adopted the value 1000 eV as the upper limit of the resolved resonance region since the existing experimental data do not allow us to identify resonances above this energy with confidence. It should be noted that, when performing the parametrization, we only used the authors' values for the cross-sections and resonance integrals; no evaluation was carried out at the parameter level. The calculations were based on the weighted mean values given in Table 1 for the thermal cross-sections and resonance integrals, which were obtained via the relevant measurements, and on experimental data for $\sigma_t(E)$, $\sigma_\gamma(E)$ and $\sigma_f(E)$ taken from EXFOR.

Table 1

Thermal cross-sections and resonance integrals for ^{244}Cm (barns)

Ref.	σ_t	σ_γ	σ_f	I_γ	I_f
[3]		25±10.3			
[4]		20			
[5]				650±50	
[6]			1±1		
[7]		14±4	1.5±1	650±50	12.5 ± 2.5
[8]	23±3				
[9]			1.1±0.5		18.03 ± 1
[10]			1±0.2		13.4 ± 1.5
[11]		15.2±1.2		626±53	
Weighted mean value	23±3	15.318±1.131	1.029±0.180	642.609±29.412	16.196±0.789

The measurements in the EXFOR library of the energy dependence of cross-sections in the region studied by us are given in Refs [2, 12–14]. It should be noted that only Ref. [2] covers the entire resolved resonance region but the quality of the cross-section measurements is very variable. Concise results of the analysis of the experimental data in question are given below:

1. $\sigma_t(E)$ – paper by Cote et al. [12], in which experimental cross-sections in the 4.3–7.80 eV range are given; owing to the low resolution, only the strong resonances to 300 eV are measured and at higher energies the cross-sections given are in fact averaged with respect to the resolution range;

2. $\sigma_\gamma(E)$ – paper by Moore and Keyworth [13], in which the cross-section is measured at the spike of bomb-shot experiment starting at 20 eV; the good energy resolution of the experiment allows these data to be used for parametrization up to 1000 eV;

3. $\sigma_f(E)$ – paper by Moore and Keyworth (see above);

   – paper by Maguire et al. [2], in which the cross-section is measured starting at 0.1 eV, but the energy resolution is such that only the data up to 20 eV can be used directly to calculate the parameters;

4. $\sigma_f(E)$ – paper by Fullwood [14], in which the fission cross-section was also measured at the spike of bomb-shot experiment, but the data were of no use for the parametrization and we did not use them.

As our starting set, we used the parameters of the most recent and most comprehensive evaluation — JENDL-3.2. This contains 67 resonances in the 10^{-5}–1000 eV range, mostly taken from Ref. [13], and one negative resonance needed to obtain the cross-section values at an energy of 0.0253 eV.

However, in our evaluation we used a scattering radius value of 8.436 fm based on the relation $R=1.35\cdot A^{1/3}$, rather than the value R=1.12 fm used in the JENDL-3.2 evaluation. The choice of the above-mentioned starting set was also motivated by the fact that, in the evaluations in ENDF/B-VI and Ref. [1], the resolved resonance region ends in the 500 eV region, and in the JEF-2 evaluation, apart from the resonance parameters to reproduce the $\sigma_t(E)$, $\sigma_\gamma(E)$ and $\sigma_f(E)$ energy dependence, more than 13 000 smooth file points are needed for each type of cross-section. It therefore makes no sense to use only the parameters of this evaluation for the calculations.

Evaluating omission of resonances for the starting set, we may conclude that there is virtually no omission due to the energy resolution and any omission of resonances can only be due to the smallness of the neutron widths. A comparison of the experimental cross-sections in Refs. [2, 12, 13] with the cross-sections calculated using the starting set parameters, taking into account the actual energy resolution in the 1–1000 eV region, showed that:

1. To obtain the resonance parameters, the data on $\sigma_f(E)$ in Ref. [2] and $\sigma_t(E)$ in Ref. [12] must be used together in the 1–20 eV range, and the data on $\sigma_t(E)$ in Ref. [12] (up to 100 eV) and $\sigma_\gamma(E)$ and $\sigma_f(E)$ in Ref. [13] in the 20–1000 eV range;

2. A number of resonance energies need to be corrected;

3. The neutron widths of the majority of the resonances are clearly too high since they were obtained in Ref. [13] by area analysis, taking Γ_γ for all resonances to be 37 meV;

4. A fairly large number of previously unidentified weak resonances can be identified and their parameters obtained, allowing the description of all the experimental data to be improved.

Fig. 1 gives experimental and calculated cross-section values, illustrating the assertions 2–4.

In this paper the resonance parameters were calculated using the shape method in several stages. First of all, using the existing experimental data in the above-mentioned energy ranges, new values were calculated for the neutron, fission and capture widths of resonances included in the starting set and, at the same time, their resonance energies were corrected.

The only assumption made here was that the values of Γ_γ for all resonances were in the 23–64 meV range and conformed to a Porter-Thomas distribution where $\upsilon \geq 40$. This range of values of Γ_γ was obtained on the basis of test calculations. A comparative analysis was then carried out of the energy dependence of the experimental and calculated cross-sections $\sigma_\gamma(E)$ and $\sigma_f(E)$, allowing a fairly large number of previously unidentified weak resonances to be identified and their resonance energies determined. After this, the neutron, fission and capture widths of these resonances were calculated and, at the same time, their resonance energies corrected. Lastly, a final corrective calculation of the parameters of all resonances in the 1–1000 eV range was performed. In the final stage, using the weighted mean values of the relevant cross-sections given in Table 1, the parameters of the negative resonance which mainly determines the cross-section values at the thermal point were calculated.

Table 2 gives the parameters we obtained for 142 resonances which adequately reproduce the experimentally measured cross-sections used for parametrization in the relevant ranges.

Table 3 gives the mean resonance parameters and thermal cross-sections calculated using our parameters. For purposes of comparison, the corresponding evaluations in ENDF/B-VI, JENDL-3.2, JEF-2 and Ref [1] are also given.

Clearly, our thermal cross-sections accurately reproduce the weighted mean values from Table 1 except for σ_t^{2200}. However, in Ref [8] no correction was made for scattering at small angles. This correction should reduce somewhat the experimentally measured value of the total cross-section at an energy of 0.0253 eV, but it cannot be calculated as the necessary information is lacking. If new measurements for σ_t^{2200} appear, it will not be difficult to perform a re-evaluation.

The main difference between our mean resonance parameters and those obtained in previous evaluations is the significantly lower values of $\langle\Gamma_n^0\rangle$, $\langle D\rangle$ and, consequently, S^0. This is due to the correction of the Γ_n^0 values for a number of previously discovered resonances, leading to a very noticeable reduction in these values, and to the large number of weak resonances first identified by us. In fact, in the JENDL-3.2 evaluation the lowest Γ_n^0 value is 0.071 meV whereas in our set of parameters it is 0.005 meV.

However, our parameters reproduce the experimentally measured cross-sections more accurately than the parameters of previous evaluations. In calculating omission of resonances for our set of parameters, we were able to conclude that, as is the case for the JENDL-3.2 set of parameters, there is virtually no omission due to the energy resolution and any omission of resonances can only be due to the smallness of the neutron widths. The evaluated values obtained for $\langle\Gamma_n^0\rangle$, $\langle D\rangle$ and S^0 are virtually the same as the values given in Table 3 and this evaluation is stable over a wide energy range.

The I_γ resonance integrals of all the evaluations given are fairly close to one another and are determined mainly by the parameters of the 7.6 eV resonance. The same cannot be said of the I_f values which, in previous evaluations, separate clearly into two groups: ENDF/B-VI and JEF-2, JENDL-3.2 and Ref [1].

Moreover, since fission for ^{244}Cm is a threshold reaction, the 1 keV–20 MeV region makes a contribution to the fission resonance integral ranging from 7.53 b (Ref. [1]) to 8.24 b (ENDF/B-VI) which, for the four evaluations given in Table 3, comprises 41.5–59.3% of the relevant I_f values for the whole region, though in terms of absolute values they agree. It is also clear from Table 3 that the two groups of evaluations mentioned above differ mainly as regards the parameters of the 7.6 eV resonance. Indeed, while the total cross-section [12] in the region of this resonance can be reproduced almost identically accurately using the parameters of ENDF/B-VI, JENDL-3.2 and this paper, the ENDF/B-VI fission cross-section evaluation is considerably higher than the only experimental measurement [2] in this region, which can be

clearly seen in Fig. 2 (the ENDF/B-VI evaluation was performed before Ref. [2] appeared). Furthermore, a comparison of fission cross-sections calculated using the parameters of JENDL-3.2 and this paper with the measurements of Ref. [2] shows that, in the 5–20 eV range, our parameters more accurately reproduce the dependence $\sigma_f(E)$ [2].

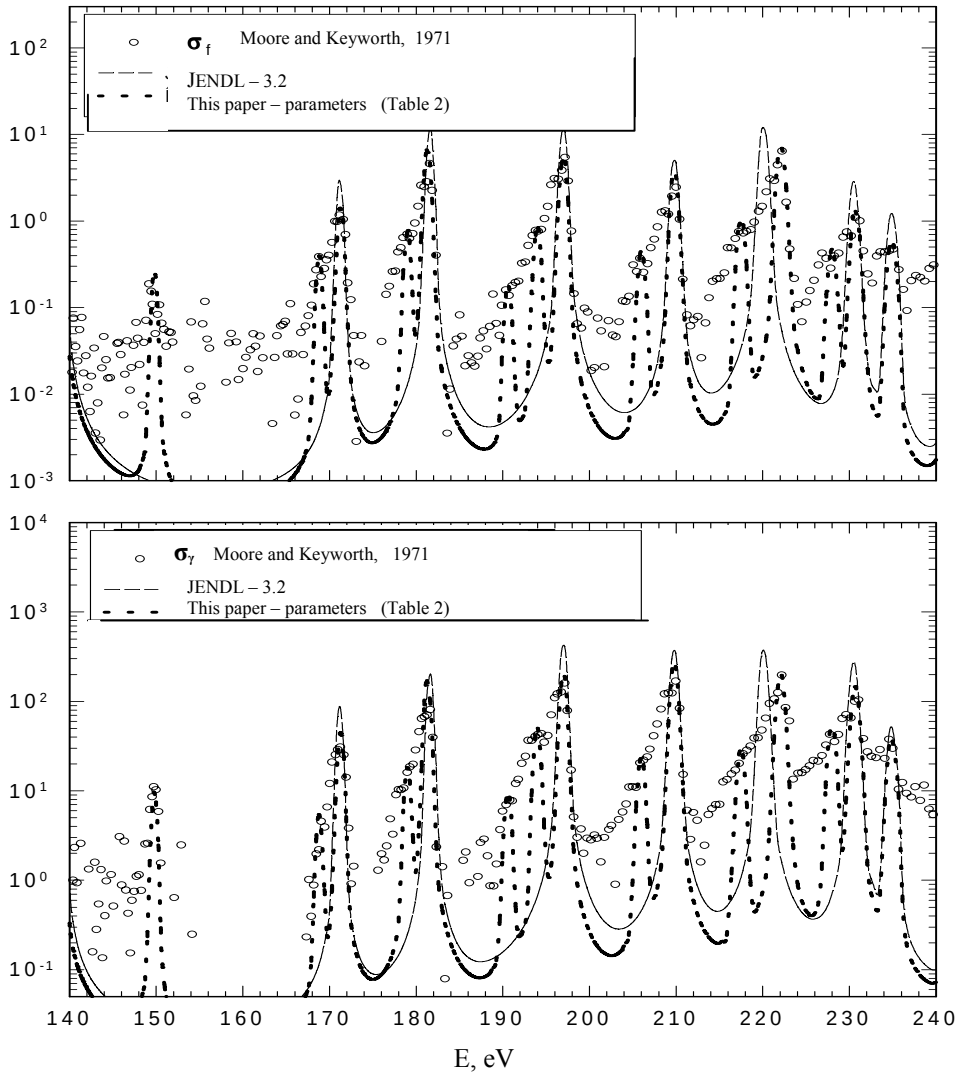

Fig. 1. Comparison of fission and radiative capture cross-sections in the 140–240 eV energy range measured experimentally [13] and calculated using the JENDL-3.2 file and the parameters in Table 2.

Table 2

Resonance parameters for ^{244}Cm

E_r,eV	Γ_n, meV	Γ_γ, meV	Γ_f, meV
-1.48	0.02451	27.78	25.838
7.57	8.7514	59.9	0.2358
12.05	0.38335	25.34	0.26378
16.79	1.5985	23.0	1.4181
22.825	0.85503	34.94	3.494
32.75	0.03241	49.6	1.1267
34.99	3.6047	39.3	2.7544
38.25	0.11613	52.38	0.34446
41.55	0.12845	53.05	0.95707
47.35	0.033	48.43	1.6613
52.78	0.59019	31.6	1.0633
66.5	0.16258	52.88	0.68306
69.95	0.43419	33.21	2.7729
85.96	23.137	34.36	0.59557
95.25	0.69328	48.39	1.66
96.12	4.1378	62.84	2.5541
123.75	0.15656	31.65	1.6886
130.75	0.67234	53.62	1.6327
132.8	6.7658	54.03	1.6878
137.0	0.31416	54.78	2.2461
138.9	1.0815	51.37	5.0085
149.8	0.2516	49.9	1.4127
168.8	0.17426	33.97	2.5381
171.3	1.6407	54.52	1.8953
179.0	0.6762	54.99	2.2966
181.3	7.978	39.52	1.4936
190.6	0.40261	49.02	0.92521
194.0	2.1867	39.2	0.62779
197.0	11.115	49.65	1.3204
206.0	1.1752	44.58	0.81858
209.8	22.225	34.89	0.49281
217.5	1.665	34.62	1.2806
222.1	14.31	61.11	2.3438
228.0	3.457	48.5	0.39806
230.7	10.212	56.98	0.54318
234.9	2.7161	32.52	0.50844
242.7	1.2991	38.66	1.605
255.25	1.3021	36.15	0.3752
260.23	1.4306	37.37	0.70521
264.9	7.8294	57.94	1.2198
272.3	3.3078	34.53	0.3406
274.25	14.093	57.44	0.61161
302.0	1.8736	47.88	0.30265
307.0	2.2256	28.34	0.09351
317.3	5.5166	36.25	0.39087
324.0	1.2251	31.23	0.65577
327.0	4.1694	57.57	1.1051
329.75	15.396	57.53	0.71581
335.0	2.2202	29.26	0.1839

E_r,eV	Γ_n, meV	Γ_γ, meV	Γ_f, meV
343.81	17.936	45.63	1.2501
353.4	27.487	62.09	2.4144
362.0	11.382	63.99	2.8449
364.8	4.1806	50.88	3.0419
378.0	3.3541	48.91	0.81874
386.5	13.179	60.87	1.9453
398.0	9.4834	43.04	0.84273
400.6	1.9113	45.98	0.27552
410.75	1.4121	42.48	1.2785
414.6	9.6196	40.25	0.31903
418.3	1.789	45.11	1.7908
421.0	50.3	39.23	1.035
427.4	7.2514	44.30	0.58621
434.0	2.1571	49.33	1.0123
440.0	2.5548	41.42	0.69254
444.0	27.532	58.77	1.53
464.0	3.256	46.0	0.35081
469.0	3.2541	46.36	0.88391
471.4	47.021	39.11	2.9922
477.0	6.5477	45.9	0.14585
489.4	10.443	43.68	0.52107
492.4	23.792	33.9	0.54671
511.45	35.145	55.22	0.25271
517.0	3.9753	47.69	0.20597
520.95	18.807	50.47	2.6575
527.0	2.4411	45.55	0.50887
531.0	2.6482	44.19	2.2491
542.0	1.7744	54.64	2.08140
544.9	1.6885	41.01	0.84155
549.75	1.8126	47.18	4.5222
565.05	2.3791	44.19	1.8078
573.0	1.7759	53.16	1.0121
580.0	3.4953	42.98	0.34548
586.0	4.7702	48.02	0.51849
592.0	3.4523	43.77	0.55695
596.4	16.926	37.36	0.67316
603.4	9.4587	28.54	0.17337
613.2	29.46	37.88	1.0238
621.0	26.574	37.85	0.81838
628.5	7.0068	36.81	0.49743
638.1	10.701	49.11	0.99788
642.0	6.4635	52.44	0.44341
648.0	38.315	40.64	1.22130
649.5	38.719	40.28	0.60474
653.0	40.144	41.28	0.09675
659.5	5.8866	51.85	0.30689
686.75	4.498	39.37	0.27976
691.3	9.9017	38.59	1.0835
696.3	15.963	37.20	0.54137
699.7	4.4588	44.16	0.75882
704.7	8.2709	43.01	4.7654
706.1	21.193	38.94	2.2079
712.8	13.454	36.1	0.19514

E_r,eV	Γ_n, meV	Γ_γ, meV	Γ_f, meV
725.5	5.4558	44.25	0.37728
731.9	4.0026	38.41	1.0593
735.1	14.16	47.83	0.21238
741.5	4.168	44.49	0.65969
746.9	4.2888	50.44	2.0091
756.0	3.5754	46.58	1.7568
762.5	57.857	27.24	0.08714
773.5	4.1981	34.12	0.26488
779.17	27.708	55.12	3.6403
791.0	4.4422	40.18	2.6312
797.5	2.9687	46.65	2.8559
803.3	2.7865	40.82	4.0135
807.0	6.4619	48.16	0.55978
817.0	6.216	47.09	4.1737
824.0	27.089	39.18	9.8479
827.0	8.8389	39.56	1.4966
843.0	16.955	45.36	0.32442
848.0	5.4277	48.45	2.5075
855.5	7.4334	42.41	0.7309
860.4	17.311	53.04	0.83916
867.2	8.2692	47.32	6.7534
874.0	12.94	46.17	0.78303
883.4	13.307	35.68	0.1458
887.0	17.078	36.56	0.49395
893.0	10.389	43.47	0.28062
900.1	3.213	50.07	1.9483
903.4	25.804	43.39	0.1296
909.0	5.6416	40.65	0.29282
913.7	12.997	54.2	1.8815
915.0	5.6347	40.7	2.3454
926.6	19.031	36.88	0.49838
947.5	5.0243	41.01	1.9468
949.5	11.332	40.84	0.62638
958.0	3.0834	40.74	0.51338
969.5	3.7091	40.73	0.51326
973.0	76.956	37.71	0.7121
979.7	9.282	42.72	0.23868
983.0	7.8108	51.79	0.23481
989.0	9.5215	39.58	0.08929
1001.3	3.7373	40.08	1.724

Table 3

Mean resonance parameters and thermal cross-sections for ^{244}Cm, calculated using the PSYCHE and INTER programs [15]

	ENDF/B-VI	JENDL-3.2	JEF-2	Evaluation in Ref. [4]	This paper
$<\Gamma_n^0>$, meV	1.616	1.834	1.894	1.982	0.4517
$<\Gamma_\gamma>$, meV	35.76	37.0	36.199	36.04	44.18
$<\Gamma_f>$, meV	1.298	1.402	2.048	1.365	1.482
σ_t, barns	17.951	27.203	22.996	27.622	22.508
σ_n, barns	6.982	11.063	7.571	11.342	6.161
σ_γ, barns	10.365	15.102	14.410	15.252	15.318
σ_f, barns	0.604	1.037	1.030	1.0287	1.029
g_γ	1.00277	1.00103	1.00806	1.00551	1.00545
g_f	0.99214	0.98932	1.00194	1.00281	0.99376
R ($\times 10^{-12}$), cm	0.906233	1.120	0.8950	0.950	0.843588
<D>, eV	14.110	14.522	14.335	14.535	7.112
S^0 ($\times 10^{-4}$)	1.176	1.282	1.341	1.401	0.640
I_γ, barns					
0.5–10 eV	507.105	571.44	551.107	553.035	552.27
0.5–2·10^7 eV	593.556	660.166	634.036	635.200	640.683
I_f, barns					
0.5–10 eV	7.183	1.96	8.192	2.171	2.279 [1)] 2.491 [2)]
10–520 eV	3.123	3.318	2.993	3.224	3.398 [1)] 4.787 [2)]
520-1000 eV	0.148	0.106	0.389	0.087	0.121 [1)] 0.289 [2)]
1000–2·10^7 eV	8.244	7.832	8.206	7.531	7.832 [3)]
0.5–2·10^7 eV	18.698	13.216	19.780	13.013	13.630 [4)] 15.399 [5)]

1) calculation using only the resonance parameters

2) calculation using the resonance parameters and the smooth file

3) JENDL-3.2 evaluation used

4) in the 0.5–1000 eV region, calculation using only the resonance parameters; above 1000 eV, JENDL-3.2 evaluation used

5) in the 0.5–1000 eV region, calculation using the resonance parameters and the smooth file; above 1000 eV, JENDL-3.2 evaluation used.

From Fig. 2 it is clear that three series of data (the experiment in Ref. [2], and the calculations of $\sigma_f(E)$ using the parameters in JENDL-3.2 and Table 2 and the energy resolution in Ref. [2]) differ systematically. The systematic discrepancy in the calculations using our parameters and the JENDL-3.2 evaluation were to be expected since the fission widths of both sets of parameters are fairly close but our resonance neutron widths are significantly smaller than in the JENDL-3.2 file, as mentioned above. The discrepancy between Ref. [2] and the evaluations in the region where the parametrization was performed using the data from Ref. [13], i.e. above 20 eV, prompts the assumption that there is a systematic difference in the fission cross-sections in the measurements in Ref.[2] and Ref. [13]. Indeed, a comparison of the fission cross-sections in Ref. [2] and Ref. [13] averaged over ranges of 50–100 eV in the 20–1000 eV region shows that there is a noticeable systematic discrepancy in these experimental data. Both series of averaged cross-sections are well interpreted by the dependence $C/\sqrt{E}$, where the value of C in Ref. [2] is 1.33 times higher than in Ref. [13]. The description of the fission evaluation in the JENDL-3.2 file indicates that the data from Ref. [2] were used up to 20 eV, the data from Ref. [13] in the 20 eV–1 keV region, the data from Ref. [2] again in the 1–100 keV region, and above that the data from Ref. [13] plus measurements from Refs [16, 17]; however, the systematic difference in the data in Refs [2, 13] was not taken into account in this evaluation. We obtained the parameters in Table 2 in a similar way, since only Ref. [13] gives a detailed fission cross-section energy dependence in the 20–1000 eV range. However, we believe that the data in Ref. [2] describe the average fission cross-section curve better than the data in Ref. [13], though it is not possible to evaluate accurately the cause of the discrepancy in these experiments. This is all the more true when we consider that the measurements in Ref. [13] were performed at the spike of bomb-shot experiment, and there could be several such reasons. Therefore, we did not renormalize the experimental data but calculated an addition to the fission cross-section, the so-called smooth file, to bring the $\sigma_f(E)$ values measured in Ref. [2] into agreement with the values calculated using our parameters taking into account the energy resolution in Ref. [2]. The fission cross-sections in this smooth file are given in Table 4. It turned out that only 38 points need to be used in the resolved resonance region (10^{-5}–1000 eV) to make the fission cross-section calculation agree with the experiment in Ref. [2], as is clearly shown in Fig 2. Moreover, the integral fission resonance values calculated using the measurements in Ref. [2] and the data in Tables 2 and 4 in the 0.5–1000 eV region virtually coincide, and the calculated value of I_f for the 0.5 eV–20 MeV range is increased by 1.769 b thanks to the smooth file and agrees better with the weighted mean value (see Tables 1 and 3).

Thus, the resonance parameters we obtained permit a fairly reliable representation of the energy dependences of $\sigma_t(E)$, $\sigma_\gamma(E)$ and, using the smooth file, $\sigma_f(E)$ in the 10^{-5}–1000 eV energy range.

Table 4

Smooth file for the parameters in Table 2

E_i, eV	$\Delta\sigma_f$, barns	E_i, eV	$\Delta\sigma_f$, barns	E_i, eV	$\Delta\sigma_f$, barns
10^{-5}	0.0	33.111	0.5139	95.525	0.5069
0.145	0.02	34.108	0.6943	105.69	0.3618
0.224	0.0271	37.199	0.0908	146.57	0.4489
0.689	0.0202	38.395	0.3026	155.55	0.3814
2.961	0.111	42.084	0.1984	217.36	0.4822
5.204	0.3	43.480	0.3594	234.31	0.3222
5.702	0.0	49.761	0.4818	325.04	0.2456
18.654	0.0	51.556	0.6438	391.84	0.2967
20.50	0.3249	55.345	0.4316	663.04	0.2169
22.243	0.7963	59.732	0.5368	809.60	0.3007
27.029	0.6385	69.901	0.3984	936.22	0.2499
30.02	0.6377	79.473	0.5287	1000.0	0.2702
32.214	0.75	83.062	0.3921		

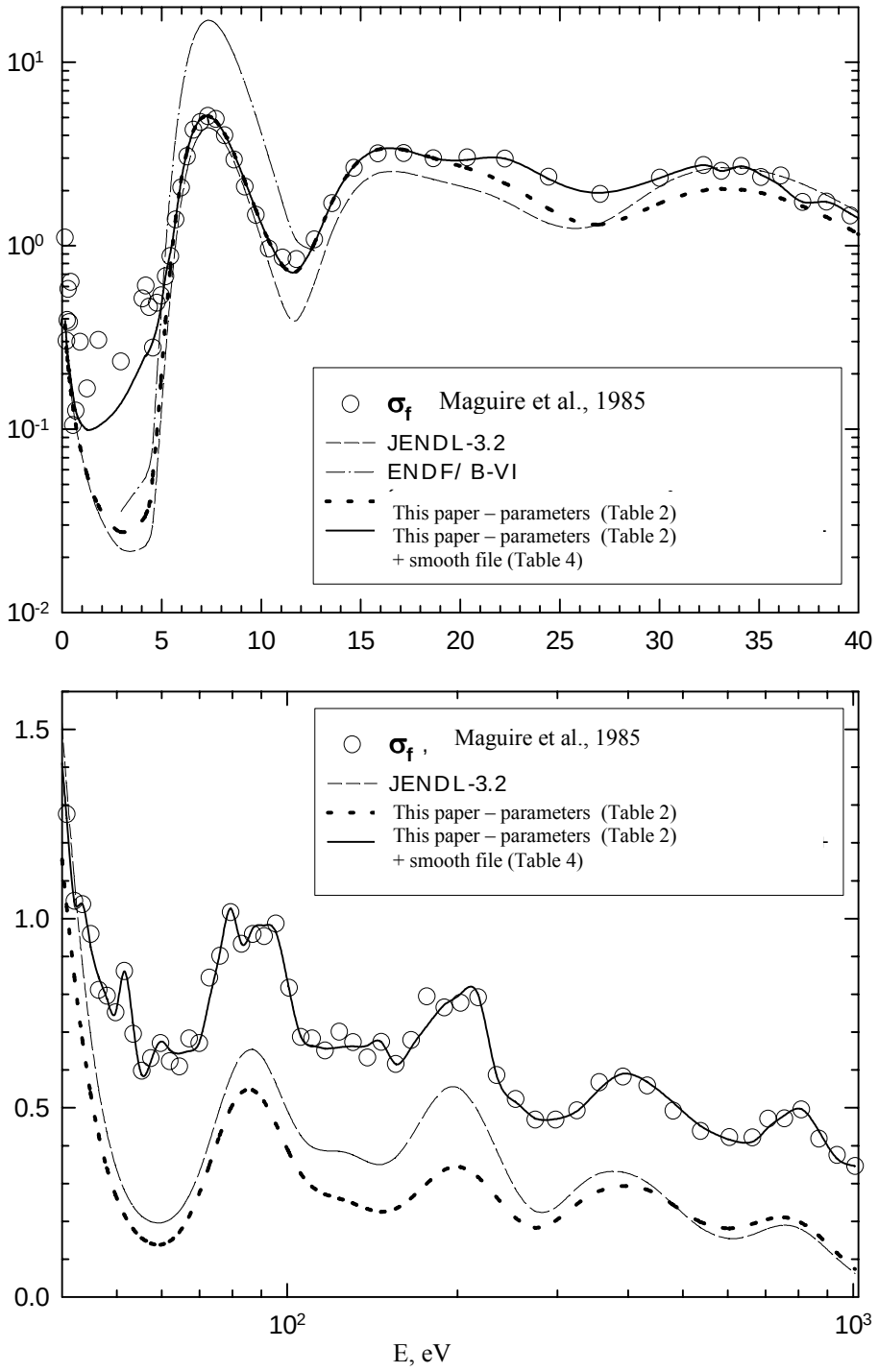

Fig. 2. Comparison of the experimentally measured fission cross-sections in Ref. [2] and cross-sections calculated using the ENDF/B-VI and JENDL-3.2 files and the results of this paper in the 10^5-1000 eV energy range.

REFERENCES

1. Klepatskij, A.B., Kolesov, A.M., Maslov, V.M., et el., Preprint IYaEh AN BSSR, 1989, No. 1 [in Russian].
2. Maguire Jr. H.T., Stopa, C.R.S., Block, R.C., et al., Nucl. Sci. Eng., 1985, V. 89, p. 293.
3. Stevens, C.M., Studier, M.H., Fields, P.R., et al., Phys. Rev., 1954, V. 94, p. 974.
4. Ice, C.H., Report DP-MS-66–69, 1969.
5. Schuman, R.P., Report WASH-1136, 1970, p. 54.
6. Kroshkin, N.I., Zamyatnin, Yu.S., Atomnaya Ehnergiya, 1970, V. 29, No. 2, p. 95 [in Russian].
7. Thompson, M.S., Hyder, M.L., Rucland, R.J., Journal of Inorganic and Nuclear Chemistry, 1971, V. 33, No. 6, p. 1553.
8. Berreth, J.R., Simpson, F.B., Rusche, B.C., Nucl. Sci. Eng., 1972. V. 49, p. 145.
9. Benjamin, R.W., MacMurdo, K.W., Spencer, J.D., Nucl. Sci. Eng., 1972, V. 47, p. 203.
10. Zhuravlev, K.D., Kroshkin, N.I., Chetverikov, A.P., Atomnaya Ehnergiya, 1975, V. 39, No. 4, p. 285 [in Russian].
11. Gavrilov, V.D., Goncharov, V.A., Atomnaya Ehnergiya, 1978, V. 44, No. 3, p. 246 [in Russian].
12. Cote, R.E., Barnes, R.F., Diamond, H., Phys. Rev. B, 1964, V. 134, p. 1281.
13. Moore, M.S., Keyworth, G.A., Phys. Rev. C, 1971, V. 3, p. 1656.
14. Fullwood, R.R., McNally, J.H., Shunk, E.R., Neutron Cross Sections and Technology: Proc. of a Conf., 1968, Washington, V. 1, p. 567.
15. Danford, C.L., ENDF Utility Codes Release 6.9, IAEA-NDS-29, 1993
16. Fomushkin, Eh.F., Novoselov, G.F., Vinogradov, Yu.I., et al., Yadernaya Fizika, 1980, V. 31, No. 1, p. 39 [in Russian].
17. Vorotnikov, P.E., Kozlov, L.D., Molchanov, Yu.D., Atomnaya Ehnergiya, 1984, V. 57, No. 1, p. 61 [in Russian].

04-34911 (209) [3]
Translated from Russian

UDC 539.17

EFFECTIVE REACTION CROSS-SECTIONS FOR ^{7}Be PRODUCTION BY INTERACTION OF FAST NEUTRONS IN AN ACCELERATOR-DRIVEN SYSTEM WITH LIGHT NUCLEI

V.S. Buttsev[1], T.N. Korbut[2], S.V. Korneev[3], B.A. Martsynkevich[2], A.M. Khil'manovich[2], S.E. Chigrinov[3], D. Chultehm[1]
[1]Joint Institute for Nuclear Research, Dubna, Russia
[2]B.I. Stepanov Institute of Physics, Belarus National Academy of Sciences, Minsk, Belarus
[3]Sosny Joint Institute for Energy and Nuclear Research, Belarus National Academy of Sciences, Minsk, Belarus

EFFECTIVE REACTION CROSS-SECTIONS FOR ^{7}BE PRODUCTION BY INTERACTION OF FAST NEUTRONS IN AN ACCELERATOR-DRIVEN SYSTEM WITH LIGHT NUCLEI. The measurement of effective reaction cross-sections for $^{7}_{4}$Be production by irradiation of light nuclei (C, O, F, Na, Cl, K) with fast neutrons from the interaction of 660 MeV protons with a thick lead target is described. The experiment was conducted on the proton accelerator at the Nuclear Problems Laboratory (JINR, Dubna). Measurements of the neutron flux density and the $^{7}_{4}$Be production rate were performed using the activation method. Cross-sections of $^{7}_{4}$Be production decrease from 0.01 barns for carbon to 0.00005 barns for potassium. The model of nuclear reactions of ~20–50 MeV neutrons with light nuclei taking into account the effective potential barrier for $^{7}_{4}$Be was used. In general, the model correctly reproduces the measured values.

Introduction

In recent years, there have been intensive developments in the design of energy systems based on a combination of high-energy reactions involving the spallation and fission of heavy nuclei (ADS) [1, 2]. The main feature of this technology is the use of subcritical systems (k_{eff}<1) controlled by proton accelerators producing protons with energies of the order E_p~1–2 GeV. This approach assumes that a high-energy proton beam interacts with a neutron-generating target (Pb, Bi, W and Pb-Bi) and the neutrons formed as a result of the development of a nucleon-meson cascade are multiplied by a subcritical reactor system with a multiplication factor of M=1/(1-k_{eff}) ≈50. It is assumed that in such systems a neutron flux density of F ~10^{15} neutrons/cm^2·s can be achieved, providing a basis for both energy production and large-scale transmutation of long-lived fission fragments and minor actinides. Among the possible plans for such systems, approaches employing fluoride salts of light and heavy metals, such as LiF, NaF, BeF_2, ZnF_2, NaF-ZnF_2 and Li-Pb, as coolants have recently been widely discussed. Moreover, the transuranium elements also dissolve fairly well in these salts, so we can consider using only subcritical molten salt blankets controlled by high-energy accelerators [3].

A distinctive feature of ADS technology is the generation in the system of neutrons with an energy distribution ranging from an electronvolt to several hundred megaelectronvolts. In contrast to normal critical systems, this generates a wider spectrum of radioactive nuclei [4] with fairly long half-lives through spallation reactions. The formation of such isotopes give rise to an additional radiation burden, especially in systems employing molten salts. One such reaction on light nuclei is the reaction where a final-state ^{7}Be

nucleus is formed whose half-life is 53.3 days and whose transition to ground state is accompanied by the emission of a γ-ray with an energy of E_γ = 477.6 keV.

We measured the ^{7}Be yield cross-section in water in a spectrum of neutrons generated in a nucleon-meson cascade in a lead target irradiated with a 900 MeV proton beam as part of a series of experiments to determine the total neutron yield [5, 6], and the paper is a continuation of a cycle of experiments on ADS technology and deals with the experimental measurement of the cross-section of ^{7}Be production on light nuclei (C, O, F, Na, Cl, K) in reactions induced by neutrons produced in a neutron-generating target made of Pb irradiated with 660 MeV protons.

It should also be noted that, for light nuclei (A<50) with a half-life ranging from a few months to several years, all other characteristics being the same, the dose rate P and the dose D due to ^{7}Be formation can be significant.

Indeed, according to the activation equation, the number of decays of nuclei of the i-th type occurring over the time t $N_i(t)$ is related to the other nuclear physics characteristics in the following way:

$$N_i(t) = \frac{mk_i N_A}{M\lambda_i}\left[1-\exp(-\lambda_i t_a)\right]\exp(-\lambda_i t_s)\left[1-\exp(-\lambda_i t)\right]\int_{E_i}^{E^{\max}}\sigma_i(E)\varphi(E)dE. \quad (1)$$

Here, m is the mass of the irradiated element, M is its atomic mass, N_A is the Avogadro number, k_i is the isotope content in the sample on which nuclei of the i-th type are formed, λ_i is the radioactive decay constant of nuclei of the i-th type, t_a, t_s and t are the time the substance was subjected to neutron activation, the cooling time after irradiation and the time of the subsequent radiation impact of the radionuclide formed respectively, $\sigma_i(E)$ is the cross-section of the reaction leading to the formation of nuclei of the i-th type and $\varphi(E)$ is the spectral density of the flux of neutrons of energy E. As we know, the radiation dose D_i is proportional to the number of decays N_i

$$D_i(t) = aK_{\gamma i}N_i(t). \quad (2)$$

In formula (2), $K_{\gamma i}$ – K-gamma – is the γ-ray constant of the i-th nuclei contributing to the radiation dose, and a is a coefficient which takes account of the location of the radionuclide source relative to the irradiated object.

Expression (1) contains a combination of time factors

$$B_i = \frac{\left[1-\exp(-\lambda_i t_a)\right]\exp(-\lambda_i t_s)\left[1-\exp(-\lambda_i t)\right]}{\lambda_i}, \quad (3)$$

which take account of the half-life of the product nucleus and the time characteristics of the activation of the substance by the neutrons and the subsequent decay of the nuclei. Table 1 gives the values of the time parameter B for radionuclides with different half-lives for the situation where $t_a = t$ and minimum cooling after activation.

Table 1

Time parameter *B* relative to the half-life and time *t*

\ \ *t*, s \ $T_{1/2}$, s \	*B*					
	10^5 ≈ 1.16 days	10^6 ≈ 11.6 days	$4.61 \cdot 10^6$ ≈ 53.3 days	10^7 ≈ 116 days	$3.16 \cdot 10^7$ ≈ 1 year	10^8 ≈ 3.16 years
10^5 ≈ 1.16 days	$3.61 \cdot 10^4$	$1.44 \cdot 10^5$	$1.44 \cdot 10^5$	$1.44 \cdot 10^5$	$1.44 \cdot 10^5$	$1.44 \cdot 10^5$
10^6 ≈ 11.6 days	$6.49 \cdot 10^3$	$3.61 \cdot 10^5$	$1.33 \cdot 10^6$	$1.44 \cdot 10^6$	$1.44 \cdot 10^6$	$1.44 \cdot 10^6$
$4.61 \cdot 10^6$ ≈ 53.3 days	$1.48 \cdot 10^3$	$1.29 \cdot 10^5$	$1.67 \cdot 10^6$	$4.02 \cdot 10^6$	**$6.55 \cdot 10^6$**	$6.67 \cdot 10^6$
10^7 ≈ 116 days	$6.89 \cdot 10^2$	$6.49 \cdot 10^4$	$1.08 \cdot 10^6$	$3.61 \cdot 10^6$	**$1.14 \cdot 10^7$**	$1.44 \cdot 10^7$
$3.16 \cdot 10^7$ ≈ 1 year	$2.21 \cdot 10^2$	$2.15 \cdot 10^4$	$4.22 \cdot 10^5$	$1.77 \cdot 10^6$	**$1.14 \cdot 10^7$**	$3.60 \cdot 10^7$
10^8 ≈ 3.16 years	$6.93 \cdot 10^1$	$6.89 \cdot 10^3$	$1.43 \cdot 10^5$	$6.47 \cdot 10^5$	$5.58 \cdot 10^6$	$3.60 \cdot 10^7$
10^9 ≈ 31.6 years	$6.93 \cdot 10^0$	$6.93 \cdot 10^2$	$1.47 \cdot 10^4$	$6.89 \cdot 10^4$	$6.77 \cdot 10^5$	$6.47 \cdot 10^6$
10^{10} ≈ 316 years	$6.93 \cdot 10^{-1}$	$6.93 \cdot 10^1$	$1.47 \cdot 10^3$	$6.93 \cdot 10^3$	$6.91 \cdot 10^4$	$6.89 \cdot 10^5$

From Table 1 it is clear that, for operation of subcritical systems over a period of time of $t \approx 1$ year, the values of the time parameter *B* have a maximum for radionuclides with a half-life of $T_{1/2} \sim 10^7$–$3.16 \cdot 10^7$ s. For this period of time *t*, the time parameter *B* of the radionuclide ^{7}Be ($T_{1/2}$=53.3 days) is close to the maximum value (~60%), therefore the radionuclide ^{7}Be poses a radiation risk. Apart from ^{7}Be, there may be an additional radiation burden from ^{22}Na ($T_{1/2}$ = 2.602 years), and ^{3}H ($T_{1/2}$ = 12.43 yrs) and ^{14}C ($T_{1/2}$ = 5717 years).

We noted above that, in subcritical systems controlled by high-energy accelerators, the presence of high-energy neutrons leads to the formation of nuclei with a high reaction threshold energy value. As an example, Table 2 gives the threshold energies for ^{7}Be production on ^{12}C, ^{16}O, ^{19}F, ^{23}Na, ^{35}Cl and ^{39}K. As we can see, the threshold energy values lie in the 15–27 MeV range, i.e. in a neutron flux energy region comprising a significant proportion of the overall neutron spectrum.

Table 2

Reaction threshold energies *T* for production of ^{7}Be by interaction of neutrons with carbon, oxygen, fluorine, sodium, potassium and chlorine nuclides

Reaction	*T*, MeV
$^1_0n + ^{12}_6C \rightarrow ^7_4Be + ^6_2He$	27.40
$^1_0n + ^{16}_8O \rightarrow ^7_4Be + ^{10}_4Be$	26.61
$^1_0n + ^{19}_9F \rightarrow ^7_4Be + ^{13}_5B$	27,10
$^1_0n + ^{23}_{11}Na \rightarrow ^7_4Be + ^{17}_7N$	26.19
$^1_0n + ^{35}_{17}Cl \rightarrow ^7_4Be + ^{29}_{13}Al$	19.03
$^1_0n + ^{39}_{19}K \rightarrow ^7_4Be + ^{33}_{15}P$	15.56

Measuring the cross-section ^{7}Be yield from light nuclei is also of some interest for studying the characteristics of the nuclear reaction mechanism where heavy fragments are formed in the final state, since there is no consistent theory for describing such reactions.

The experiment

Set-up of the experiment. The experiments were conducted using the proton beam of the phasotron at the Nuclear Problems Laboratory of the Joint Institute for Nuclear Research. The 660 MeV proton beam was incident on a cylindrical lead target 8 cm in diameter and 40 cm long. The diameter of the proton beam on the lead target was 3 cm. Over an exposure time of 25 hours the proton fluence was $5.5 \cdot 10^{13}$.

The targets to be irradiated (water, heavy water, polyethylene, graphite, fluoroplastic, sodium chloride and potassium chloride) were positioned on the lateral surface of the lead cylinder (see Fig. 1). The targets were placed in cylindrical polyethylene containers 76 mm in diameter and 36 mm high.

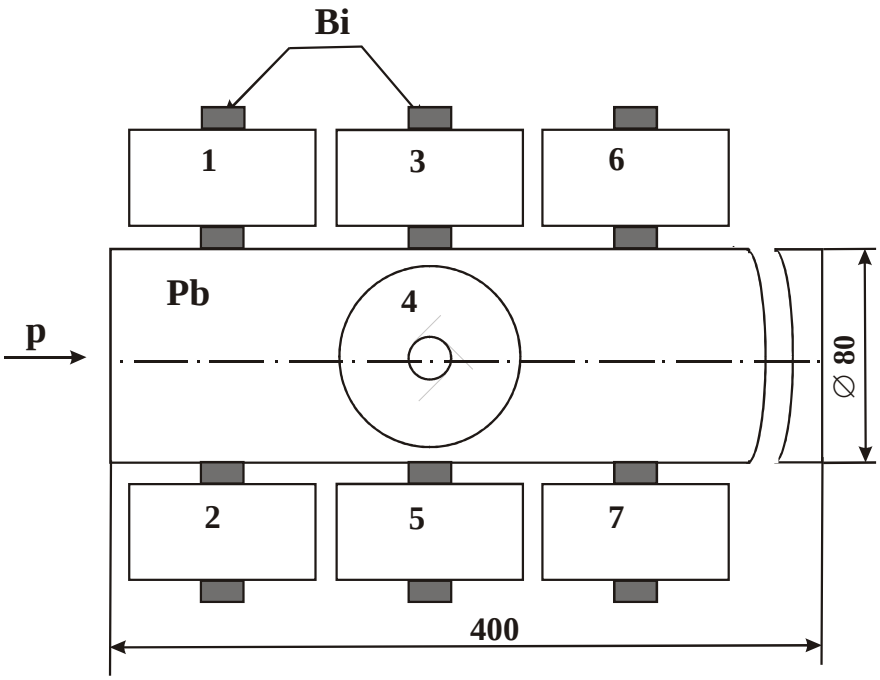

Fig. 1. Diagram of the experiment. In the figure, the substance samples are designated as follows: 1 – H_2O; 2 – D_2O; 3 – CH_2; 4 – C; 5 – CF_2; 6 – NaCl; 7 – KCl.

Leakage neutrons formed in a series of spallation reactions were monitored for the reactions ^{209}Bi(n,3n)^{207}Bi, ^{209}Bi(n,4n)^{206}Bi, ^{209}Bi(n,5n)^{205}Bi, ^{209}Bi(n,6n)^{204}Bi and ^{209}Bi(n,7n)^{203}Bi, with the thresholds 14.44 MeV, 22.45 MeV, 29.62 MeV, 38.09 MeV and 45.31 MeV respectively. Bi monitors weighing approximately 8 g were placed on the end surfaces of the polyethylene containers (Fig. 1). From the measured activation integrals and the known cross-sections of the ^{209}Bi (n, xn) reaction [8], the neutron flux density F above the threshold energy was determined. The experimental values for the speeds of the threshold reactions on bismuth and the neutron flux density values agree well with the results of calculations made using codes employing the Monte Carlo method [7].

Additional monitoring of the uniformity of the neutron flux density was performed by taking comparative measurements of ^{7}Be activity in empty polyethylene containers.

After being irradiated with neutrons, the substances were put into unirradiated containers. The γ-radiation spectra were measured using a low-background, high-efficiency, semiconductor HPGe spectrometer with an 80% registration efficiency relative to NaI(Tl). The irradiated substances were placed 10 cm above the detector. The activity was recorded for 1–3 days. To take account of a possible background contribution to the E_γ=477.6 keV photopeak region, the γ-spectrum of unirradiated substances was recorded

under the same conditions. The processing of the background spectra showed that there was no peak in the 477.6 keV energy region.

Figure 2 shows a fragment of a typical γ-radiation spectrum of a sample. The relative statistical error of the number of counts in the peak for H_2O, D_2O, C, CH_2 and CF_2 was 0.5–1.0%, and for NaCl and KCl it was ~2.0%.

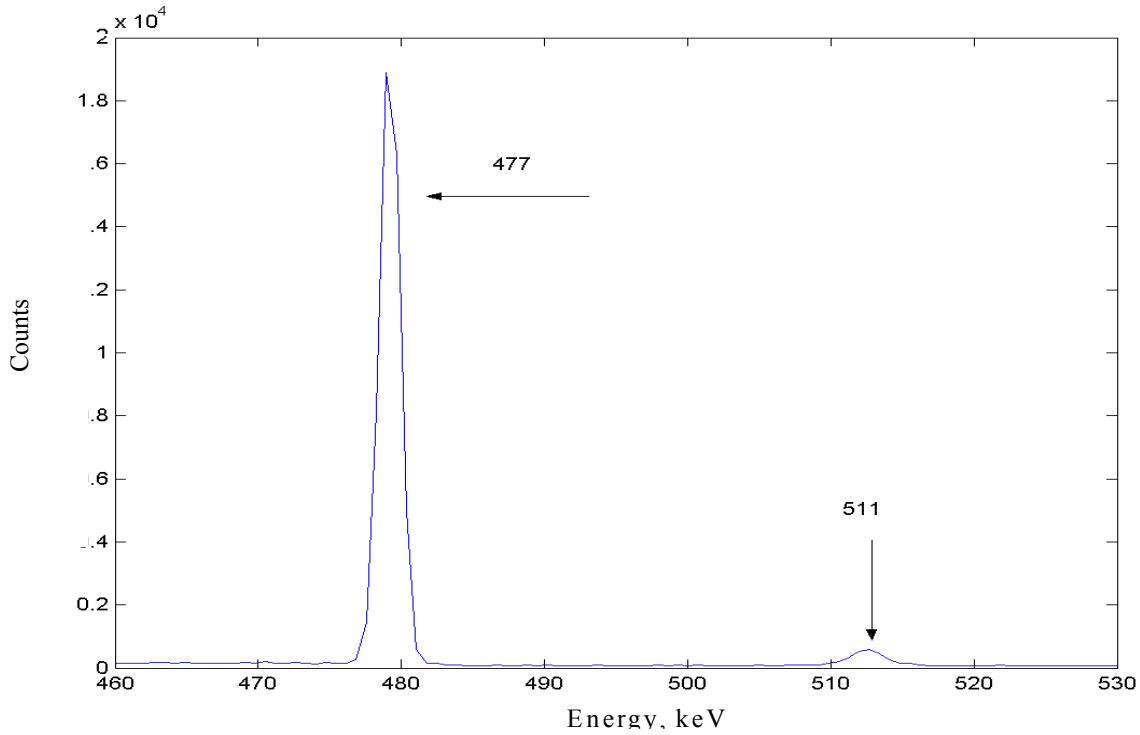

Fig. 2. Fragment of a typical γ-radiation spectrum of irradiated samples (carbon sample — graphite)

Experimental results The value measured in the experiment is the specific activity A of the radionuclide ^{7}Be in the chemical substance when irradiation with neutrons ceased

$$A = \frac{S}{m\varepsilon\, \rho exp(-\lambda t_s)[1-\exp(-\lambda t_m)]/\lambda}, \qquad (4)$$

where S is the number of counts in the analytical peak, m is the mass of the chemical substance, ε is the E_γ=477.6 keV γ-ray registration efficiency taking into account self-absorption in the sample, p is the number of E_γ=477.6 keV γ-rays per ^{7}Be decay, and t_s and t_m are the substance cooling time after neutron activation and the induced activity measurement time respectively.

Table 3 gives the values of the specific ^{7}Be activities in the substances being studied after irradiation with neutrons.

The specific ^{7}Be activity ascribed to a chemical element A_0 is calculated by taking into account the content by mass of this element in the chemical substance k and the specific activity value of the substance A.

Analysis of results

The specific activity of the fluorine in the fluoroplastic was calculated taking into account the measured activity of the carbon (graphite). To determine the activities of the Na and Cl in the sodium

chloride and the K and Cl in the potassium chloride, the ratios of the ^{7}Be production cross-sections σ(Na)/σ(Cl) or σ(Cl)/σ(K) (see formulae (8)–(9) below) were used; these were calculated taking into account the penetrability of the effective potential barrier. Here, the calculated and measured activity values for sodium chloride and potassium chloride agree with one another.

The speed of the ^{7}Be production reaction when fast neutrons interact with an element

$$I = \int_T^{E^{\max}} \sigma(E)\varphi(E)dE \tag{5}$$

is linked to the specific activity A_0 due to the element as follows:

$$A_0 = \frac{N_A}{M}[1 - \exp(-\lambda t_a)]I. \tag{6}$$

The unknown value (averaged with respect to the reaction cross-section neutron spectrum $<\sigma(E)>$) is calculated as

$$\langle\sigma(E)\rangle = \frac{I}{F}, \tag{7}$$

where F is the neutron flux density above the threshold energy T (see Table 2). As is shown in Ref. [9], the shape of the cross-sections of high-energy neutron nuclear reactions is slightly dependent on the mass number of the target nucleus. Therefore, the neutron flux densities F above the ^{7}Be production threshold energies were determined by interpolating the flux density values for threshold reactions on bismuth which are close in terms of energy.

Table 3

Specific ^{7}Be activities of irradiated substances *A*

No.	Substance	Chemical formula	Mass of sample g	Specific ^{7}Be activity of substance A, Bq/g
1	Water	H_2O	104.0	1.74±0.05
2	Heavy water	D_2O	120.3	1.43±0.05
3	Polyethylene	CH_2	117.5	10.55±0.25
4	Graphite	C	207.5	7.82±0.2
5	Fluoroplastic	CF_2	241.6	2.69±0.07
6	Sodium chloride	NaCl	127.0	0.47±0.01
7	Potassium chloride	KCl	111.0	0.21±0.01

In this study, the results were interpreted using the following model. It is assumed that the reaction cross-section for ^{7}Be production by interaction of a fast neutron of energy E ~10 MeV higher than the threshold with the nucleus (A, Z) can be written as follows:

$$\sigma_i(A,E) = \pi R^2 \eta_i, \tag{8}$$

where R is the radius of the nucleus and η_i is the probability of a reaction in the channel i. The reaction probability η_i was written in a form similar to that used in Ref. [10]:

$$\eta_i = c_i D(R, \mu_i, z_i, Z, E). \tag{9}$$

Here, $D(...)$ is the penetrability of the effective potential barrier of the nucleus (A, Z) for ^{7}Be with the charge z_i=4 and the reduced mass μ_i, and c_i is the probability of the formation of the configuration i in the compound nucleus.

The cross-section values for ^{7}Be production in the irradiated elements, averaged with respect to the fast neutron spectrum are given in table 4.

Conclusion

The ^{7}Be production cross-sections averaged with respect to the fast neutron spectrum given in Table 4 show a decrease as the mass number of the target nucleus increases. The ^{7}Be production reaction speeds, to within ~10%, are not dependent on the presence of deuterium or protium in the water. Similarly, the presence of the hydrogen in the polyethylene does not affect the speed of ^{7}Be production by interaction of fast neutrons with the carbon to within the limits of measurement error.

Analysis of the experimental ^{7}Be production cross-section values for light nuclei using a model which takes account of the penetrability of the effective potential barrier revealed a regular tendency in the dependence on the mass number A and the charge of the nucleus Z. In the case of interaction of a fast neutron with a ^{12}C nucleus, ^{7}Be production can be viewed as similar to emission of ^{6}He by a ^{13}C nucleus. For this reaction, there is clearly major deformation of the Coulomb barrier.

Comparing the cross-section value for ^{7}Be production on oxygen obtained in this study (0.0020±0.0005 barns) for E_p = 660 MeV protons incident on a lead target with the cross-section from Ref. [5] for a proton energy of E_p = 900 MeV (σ= 0.0015±0.0003 barns), we can see that they agree to within the limits of error. This conclusion corroborates the neutron spectrum calculations performed using programs based on the Monte Carlo method for primary protons of various energies. The calculated spectra, normalized to one neutron, virtually coincide. This indicates that the ^{7}Be production reaction cross-section values averaged with respect to the neutron spectrum for different proton energies must also be close to one another.

Table 4

Cross-sections for ^{7}Be production on carbon, oxygen, fluorine, sodium, chlorine and potassium averaged with respect to the fast neutron spectrum

No.	Element (substance)	Reaction cross-sections, barns; (relative error, %)
1	C(CH_2)	$1.0\cdot10^{-2}$ (23)
2	C	$6.4\cdot10^{-3}$ (23)
3	O (H_2O)	$2.0\cdot10^{-3}$ (25)
4	O (D_2O)	$1.9\cdot10^{-3}$ (25)
5	F (CF_2)	$1.4\cdot10^{-3}$ (27)
6	Na (NaCl)	* $1.5\cdot10^{-3}$ (30)
7	Cl (NaCl, KCl)	* $1.5\cdot10^{-4}$ (30)
8	K (KCl)	* $5.7\cdot10^{-5}$ (30)

Note. Reaction cross-section values obtained using formulae (8) and (9) and experimentally determined specific activity values for NaCl and KCl are marked with an asterisk (*).

In conclusion, the following may be inferred. The model used of nuclear reactions of ~20–50 MeV neutrons with light nuclei, which takes account of the effective potential barrier for the charged nucleus ^{7}Be, correctly reproduces the experimental values obtained for the ^{7}Be production cross-section overall. To obtain more accurate reaction cross-section values, particularly for ^{12}C, greater detail on the excitation mechanism would be required, which would include taking account of the structure of the initial and final states of the atomic nuclei [Ref. 11], and this is rather difficult.

The authors wish to express their gratitude for the kindness and assistance they received when conducting the work to N.A. Rusakovich and the phasotron staff at the Nuclear Problems Laboratory of the Joint Institute of Nuclear Research (Dubna).

References

1. Vasil'kov, R.G., Gol'danskij, V.I., Dzhelepov, V.P., Dmitrievskij, V.P., The accelerator-driven method of neutron generation, Atomnaya energiya, 1970, Vol. 29, No. 3, pp. 151–158 [in Russian].

2. Accelerator driven systems: Energy generation and transmutation of nuclear waste, Status report, IAEA-TECDOC-985, November, 1997.

3. K. Furukawa, S. Chigrinov, Y. Kato, K. Mitachi, Accelerator Molten-Salt Breeding Power Reactor Useful for Pu- burning and ^{233}U- Production, Seventh International Conference On Emerging Nuclear Systems, ICENES '93, 1993, pp. 429–433.

4. C. Rubbia, J.A. Rubio, S. Buono et al., Accelerator driven systems: Energy generation and transmutation of nuclear waste, Status report, IAEA-TECDOC-985, November, 1997, pp. 187–312.

5. Buttsev, V.S., Buttseva, G.L., Dudarev, S.Yu. et al., Experimental determination of the effective reaction cross-section value for ^{7}Be production by interaction of fast neutrons and water, JINR Preprint R1-2001-167, Dubna, 2001 [in Russian].

6. Martsynkevich, B.A., Khil'manovich, A.M., Korneev, S.V., et al., Reconstruction of fast neutron spectra over a wide energy range (up to 200 MeV) in the subcritical uranium-lead assembly of the Energy Plus Transmutation accelerator-driven system, JINR Preprint R1-2002-65, Dubna, 2002 [in Russian].

7. J.F. Briesmeister, MCNP — A general purpose N-particle transport code, version 4B, Report LA-12625-M, Los Alamos National Laboratory, 1997.

8. T. Nakamura et al., Proceedings of the Second Specialists Meeting on High Energy Nuclear Data (January 26–27, 1995, JAERI, Tokai, Japan), Eds. T. Fukahori and N. Kishida.

9. Barashenkov, V.S., Cross-sections for the interaction of particles and nuclei with nuclei, Dubna, JINR, 1993, 346 p [in Russian].

10. Davydov, A.S., Theory of the atomic nucleus, Moscow, Gosizdat fiz.-mat. lit., 1958, 484 p [in Russian].

11. Neudach, V.G., Smirnov, Yu.F., Nucleon associations in light nuclei, Izdatel'stvo Nauka, Moscow, 1969, 414 p, [in Russian].

Nuclear Data Section
International Atomic Energy Agency
P.O. Box 100
A-1400 Vienna
Austria

e-mail: services@iaeand.iaea.org
fax: (43-1) 26007
cable: INATOM VIENNA
telex: 1-12645
telephone: (43-1) 2600-21710

Online: TELNET or FTP: iaeand.iaea.org
username: IAEANDS for interactive Nuclear Data Information System
usernames: ANONYMOUS for FTP file transfer;
FENDL2 for FTP file transfer of FENDL-2.0;
RIPL for FTP file transfer of RIPL;
NDSONL for FTP access to files saved in “NDIS” Telnet session.
Web: http://www-nds.iaea.org